Design and Applications

of

Multi-Channel Directional Couplers

by

Ravi James McCosker

LLB BSc (Hons1)

This thesis is presented for the degree of

Doctor of Philosophy

Department of Electronic Engineering

Faculty of Science

Macquarie University

Australia

22 December 2010

Abstract

The research in this thesis presents the analysis and design of multi-channel directional coupler structures for applications in optical sensing and electro-optic devices. The structures are analysed using supermodes and a potential limitation is identified with the discovery of the phenomenon of partial image revivals. A detailed analysis is presented along with one possible exploitation of this phenomenon with the design of a compact wavelength division multiplexer.

The outcomes of the research include: i) an evanescent field optical sensor is designed using the multi-channel directional coupler structure; the design is based on the idea that the analyte to be measured infiltrates the spacing between the coupled waveguides so that the sensor can exploit the exponential dependence of the coupling on the analyte refractive index; ii) an optical chemical sensor is designed that uses silicon slot waveguides; the sensor exploits the high confinement of light in the slots, whilst retaining the exponential dependence of the coupling on the analyte refractive index; iii) discovery of the differential multi-channel directional coupler structure; and the design of a more efficient optical chemical sensor using this structure; iv) a multi-channel directional coupler refractive index sensor is design in fiber, i.e. as a dual-core microstructured optical fiber; v) a compact wavelength division multiplexer for fluorescence sensing is designed; vi) electro-optic devices including an optical electric field sensor, switch and modulators are design using the multi-channel directional coupler structure and recent electro-optic materials.

Certificate of Originality

I certify that the work in this thesis entitled "Design and applications of multi-channel directional couplers" has not previously been submitted for a degree nor has it been submitted as part of requirements for a degree to any other university or institution other than Macquarie University.

I also certify that the thesis is an original piece of research and it has been written by me. Any help and assistance that I have received in my research work and the preparation of the thesis itself have been appropriately acknowledged.

In addition, I certify that all information sources and literature used are indicated in the thesis.

Ravi J. McCosker

22 December 2010

Dedication

I dedicate this thesis to my wonderful family.

To my mother Margaret, for her loving presence in my life. Your kindness and compassion towards others has enriched my life. To my father Rod, for inspiring me to develop an analytical mind and to look for solutions from outside our usual thinking patterns. To my brother Chris, for his support and encouragement; you are very special to me.

I am eternally grateful to have you all in my life.

Acknowledgements

I would like to express sincere gratitude to my principal supervisor, Professor Graham Town whose guidance, understanding and patience helped me to successfully complete this research work.

I would also like to acknowledge my co-supervisor Professor Neil Weste; thank you for your interest in my project.

A very special thank you to my friends and PhD colleagues: Matthew Fellew, Susan Bruck and Venkata Gutta. They have helped me, one way or another, on my journey to complete a PhD. I will be forever grateful for their constant positive support and enthusiasm, and our long walks around the campus.

Finally, I would like to acknowledge the generous financial support from Macquarie University in the form of the Macquarie University Research Excellence Scholarship and the Postgraduate Research Fund.

To each of the above, I extend my deepest appreciation.

List of Original Publications

This is a thesis by publication and includes 11 professional publications that either are undergoing or have undergone the peer review process, as indicated. Unlike a traditional thesis, in a thesis by publication the involvement of collaboration colleagues is required to be clarified.

Unless otherwise stated, I had the primary responsibility for the work contained in each of these publications, which included initial conception of the work, the development of the idea into a working theory, the analysis and design of a device from this theory, and the actual writing up of the work for publication. Each publication was coauthored with my primary supervisor Professor Graham E. Town. His inclusion as coauthor reflects the fact that he provided the initial idea for the research that I have pursued, reviewed each work, and offered valuable support and guidance during the entire process.

In all cases the corresponding author is the first author, with contribution otherwise indicated by the order of authors. In the case of the two publications where I am not the primary author, my level of contribution can be summarised as assisting in the theoretical development and review of each work.

The coauthored publications in this thesis are listed below (not in temporal order):

Chapter 2:

Ravi J. McCosker and Graham E. Town, **Partial Image Revivals in a Multi-Channel Directional-Coupler**, in *Proceedings of the SPIE*, 2010, vol. 7604, pp. 76040G1-10.

Ravi J. McCosker and Graham E. Town, **Multi-Channel Directional Coupler for WDM in Fluorescence Sensing**, submitted to *IEEE Journal of Lightwave Technology*.

Chapter **3**:

Ravi J. McCosker and Graham E. Town, **Multi-Channel Directional Coupler as an Evanescent Field Optical Sensor**, *Sensors and Actuators B* 150 (2010), pp. 417-424.

Ravi J. McCosker and Graham E. Town, **Optical Chemical Sensor using a Multi-Channel Directional Coupler with Slot Waveguides**, in *Proceedings of the International Conference on Photonics (ICP)*, Langkawi, 2010, pp. 1-5.

Ravi J. McCosker and Graham E. Town, **Optical Chemical Sensor using a Differential Multi-Channel Directional Coupler with Slot Waveguides**, submitted to *Sensors and Actuators B*.

Graham E. Town, **Ravi McCosker**, Wu Yuan, and Ole Bang, **Design of Microstructured Waveguide Devices for Applications in Optical Sensing**, in *Proceedings of the Optics & Photonics Congress, Advanced Photonics & Renewable Energy*, Karlsruhe, 2010.

Graham E. Town, Wu Yuan, **Ravi McCosker** and Ole Bang, **Microstructured Optical Fiber Refractive Index Sensor**, *Optics Letters* 35 (2010), pp. 856-858.

Chapter **4**:

Ravi J. McCosker and Graham E. Town, **Optical Electric Field Sensor using a Multi-Channel Directional Coupler**, submitted to *IEEE Sensors Journal*.

Ravi J. McCosker and Graham E. Town, **An Electro-Optic Switch Based on a Multi-Channel Directional Coupler**, in *Proceedings of the 35th Australian Conference on Optical Fibre Technology (ACOFT)*, Melbourne, 2010.

Ravi J. McCosker and Graham E. Town, **A Delta-K Electro-Optic Polymer Modulator using a Multi-Channel Directional Coupler**, in *Proceedings of the International Conference on Electromagnetics in Advanced Applications (ICEAA)*, Sydney, 2010, pp. 859-862.

Ravi J. McCosker and Graham E. Town, **An Electro-Optic Modulator using a Multi-Channel Directional Coupler with a Poled Electro-Optic Polymer**, in *Proceedings of the Third International Conference on Communications and Electronics (ICCE)*, Nha Trang, 2010, pp. 329-334.

Table of Contents

List of Figures

Abbreviations

DMCDC	Differential multi-channel directional coupler
MCDC	Multi-channel directional coupler
WDM	Wavelength division multiplexer

A journey of a thousand miles
must begin with a single step.

Lao Tzu,
Tao Te Ching

1

Introduction

1.1 Background

1.1.1 Integrated Optics

The concept of 'integrated optics' emerged in the late 1960s, and represented the replacement of electrical wires and wireless links with optical fibers, and later the replacement of electrical integrated circuits with photonic integrated circuits [Hunsperger, 2009]. During the late 1970s, several developments combined to bring integrated optics out of the laboratory and into the domain of practical application, i.e. the development of low-cost optical fibers and connectors; the creation of reliable con-

tinuous wave laser diodes; and the realisation of photolithographic microfabrication techniques capable of submicron linewidths [Hunsperger, 2009]. In the 1980s, optical fibers predominantly replaced electrical wires in telecommunications, and a number of manufacturers started producing optical integrated circuits for various applications [Hunsperger, 2009]. Since the 1990s a continuing impetus to the development of new integrated optic devices and systems has been the implementation of worldwide communications and data banks using computer networks such as the Internet [Hunsperger, 2009]. In such cases, the enormous bandwidths requirements of these multichannel transmission systems have only been achieved with the implementation of this technology in integrated optic devices and systems.

Paralleling these historical developments was the availability of improved fabrication methods, which also simulated the development of new integrated optic devices. For example, microtechnology (micrometer sized features) has evolved into nanotechnology (nanometer sized features) and lead to the development of nanophotonics.

Various methods of waveguide fabrication exist. One of the earliest methods is deposition of thin films. In this case, deposition is used as a general term that includes liquid-source deposition, such as spinning or dipping, as well as vacuum-vapor deposition and sputtering. The thin films can include dielectric material, e.g. lithium niobate, as well as more recently glass and polymer. Alternatively, epitaxial growth is used as a more versatile method of fabricating waveguides where a monolithic optical integrated circuit is formed on a semiconductor substrate, such as silicon or gallium arsenide [Hunsperger, 2009].

Essentially all integrated circuits are fabricated using microfabrication [Moreau, 1988]. Microfabrication uses a variety of patterning techniques, the most powerful of these

is photolithography. Photolithography is a process used to selectively remove parts of a thin film or the bulk of a substrate. Although photolithography is the dominant technology, it is not always the best, e.g. it is an expensive technology; it is poorly suited for patterning nonplanar surfaces; and it is directly applicable only to a limited set of photosensitive materials [Xia and Whitesides, 1998]. Nor is it the only option, with alternate strategies, such as soft lithography. Soft lithography represents a non-photolithographic, convenient, effective, and low-cost strategy, where an elastomeric stamp with patterned relief surface structures is used to generate patterns and structures with feature sizes ranging from 30 nm to 100 μm [Xia and Whitesides, 1998].

In recent years, interest in making integrated optic devices in polymer materials has grown rapidly, due mainly to cost reduction and flexibility. Semiconductor materials or dielectrics are relatively expensive and the fabrication processes used are very complex. On the other hand, polymer materials are potentially low cost and rapidly processed by direct photo patterning or reactive ion etching. Furthermore, flexibility in molecular engineering has allowed the development of polymers whose properties have been specifically designed for applications such as waveguides and electro-optic effects.

1.1.2 Optical Sensing

Optical sensors have emerged as useful detection and analysis tools with a wide variety of applications in diverse fields such as medicine [Lippitsch et al., 1996], microbiology [Horváth et al., 2003], power industry [Hautefeuillea et al., 2008], environmental monitoring and defense [Pohanka et al., 2007]. When compared to traditional electronic sensors, optical sensors have attracted considerable attention with some unique ad-

vantages, such as their immunity to electromagnetic inference, they do not require a reference signal, they have the capability of performing remote sensing over wide distances, compact and large bandwidth.

Optical sensors that adopt a waveguide to confine the mode and thus optical power are based on evanescent field sensing. The evanescent field is the electric field that is associated with the guided optical wave that extends outside the waveguide into the cover and substrate mediums with an exponential attenuation described by the following decay factor

$$\exp\left(-k\sqrt{{n_c}^2\sin^2\varphi - {n_w}^2}\,z\right) \tag{1.1}$$

where k is the wavenumber, n_c is the refractive index of the analyte, n_w is the refractive index of the waveguide and φ is the angle of refraction inside the waveguide at the waveguide boundary interface.

It is the interaction of the evanescent field with the cover medium that defines the basis for guided wave optical sensing. The principle of evanescent field sensing is illustrated in Fig. 1.1.

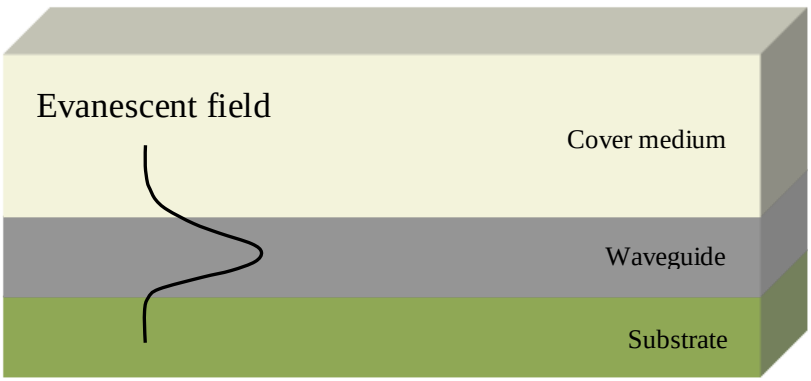

Figure 1.1: *The principle of evanescent field sensing.*

The actual transduction step may involve:

- Direct detection of a fluorescence signal induced at the surface of the waveguide (fluorescence sensing);
- detection of changes in an analyte that covers the sensing region due to an effective index change (homogeneous sensing);
- detection of chemical or biological molecules that absorb to the waveguide surface forming a thin adlayer of a specific refractive index (surface sensing).

1.1.2.1 Fluorescence Sensing

Fluorescence is the phenomenon of the photon emission by a molecule or material (fluorophore) after an initial excitation in a light-absorbing process [Demchenko, 2008]. Molecules can absorb incident radiation of a particular wavelength, moving the molecule to an excited energy level. A molecule in an excited state tends to relax to a lower energy level. If the relaxation takes place by emission of a photon without any change in spin multiplicity, the transition is known as fluorescence. The fluorescent emission can be observed usually with a longer wavelength than the excitation.

Fluorescence intensity is measured around the excitation and emission wavelengths to determine the fluorescence excitation and emission spectrum. Typically, bio-recognition molecules are labelled with fluorescent tags, such as dyes. The fluorescence indicates their presence and the interaction strength between the target and bio-recognition molecules. Alternatively, these emissions can also be characterised by the fluorescence lifetime for reporting on the fluorescent tag interactions.

Fluorescence sensing offers many attractive feature, including:

- Ultra-high sensitivity - with the detection limit of the fluorescent dye is down to a single molecule [Moerner, 2007]. This feature is important if the analyte exists in trace amounts.
- Fluorescence has a high speed of response - limited only by the fluorescence lifetime and the speed of the photochemical event that produces the response. For organic dyes this typically ranges from picoseconds to nanoseconds.
- Very high spatial resolution - with a limit around 500 nm in visible light.
- Non-destructive and non-invasive - fluorescent dye and detector instrument are separated and connected by the propagation of light.

1.1.2.2 Homogeneous and Surface Sensing

In the case of homogeneous sensing, a change in analyte refractive index Δn_a results in a change in the effective index Δn_{eff} and is given by [Passaro et al., 2007]:

$$\Delta n_{\text{eff}} = \frac{2 n_a \Delta n_a}{\eta_0 P} \iint_R \left| \boldsymbol{E}(x,y) \right|^2 dx dy \tag{1.2}$$

where η_0 is the impedance of free space, $\boldsymbol{E}$ is the electric field vector, P is the power in the optical waveguide and R indicates the analyte region.

Alternatively, in the case of surface sensing the presence of the analyte will result in a change in the thickness of the adlayer ρ. In this case, the effective index n_{eff} is given by

[Passaro et al., 2007]:

$$\Delta n_{\text{eff}} = \frac{n_{ml}^2 - n_a^2}{\eta_0 P} \iint_M \left| \boldsymbol{E}(x,y) \right|^2 dx\, dy \tag{1.3}$$

These sensing methodologies rely on the overlap of the evanescent field and the cover medium on or above the waveguide surface and the electric field strength at the surface of the optical waveguide and sensing layer.

1.1.2.3 Mach-Zehnder Interferometer Structure

A commonly used structure for optical evanescent wave sensing is the Mach-Zehnder interferometer [Schipper et al., 1997; Esinenco et al., 2005; Schmitt et al., 2007], shown in Fig. 1.2.

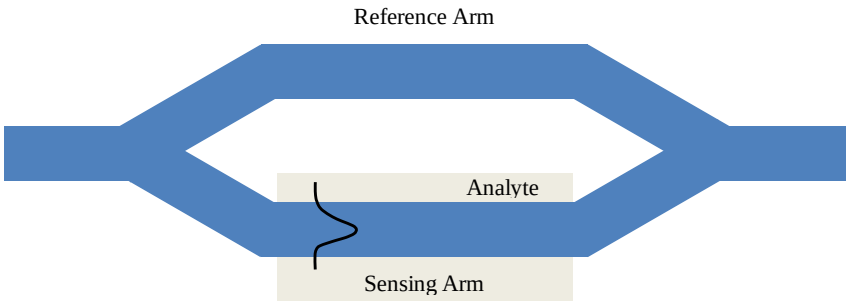

Figure 1.2: *Mach-Zehnder interferometer sensor.*

This sensor configuration shows a high sensitivity for the detection of refractive index changes on a waveguide surface within the evanescent field of the waveguide [Schipper et al., 1997]. In this configuration, the input optical field enters a Y-junction where it is split into two parts. These two fields then propagate in two separate arms. One arm is the reference arm and the other is the sensing arm. The sensing are interacts with an

analyte resulting in an accumulated phase shift $\Delta\phi$ when compared to the reference arm. Both fields are then recombined in a second Y-junction to interfere with each other. The accumulated phase difference $\Delta\phi$ is given by:

$$\Delta\phi = kL\Delta n_{\text{eff}} \tag{1.4}$$

where Δn_{eff} is the effective refractive index difference between both arms as a result of the analyte interaction; and L is the length of the sensor arms.

The sensitivity of the sensor S is given by [Passaro et al., 2007]:

$$S = -kLS_w \tag{1.5}$$

where S_w denotes the waveguide sensitivity. In the case of homogeneous sensing, waveguide sensitivity is defined as

$$S_w = \frac{\partial n_{\text{eff}}}{\partial n_a}\,; \tag{1.6}$$

and for surface sensing as:

$$S_w = \frac{\partial n_{\text{eff}}}{\partial \rho}\,, \tag{1.7}$$

where ρ denotes the thickness of the molecular adlayer.

1.1.3 Multi-Channel Directional Coupler

Consider an array of identical and equally spaced channel waveguides (Fig. 1.3). The waveguides are in sufficiently close proximity that they may be considered to be a

coupled system rather than an array of individual waveguides. Incident light focused into the input or feed waveguide will couple into the adjacent waveguides. Somekh [1974] referred to such a structure as a multi-channel directional coupler (MCDC).

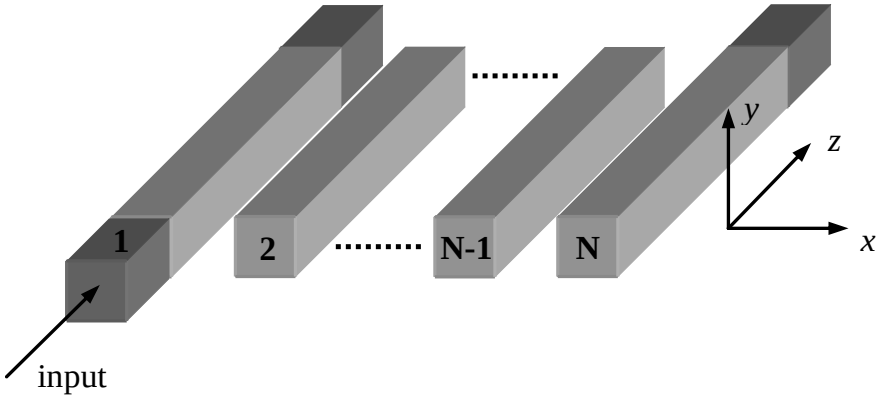

Figure 1.3: *Schematic of a side-fed N-channel multi-channel directional coupler.*

The coupling between the array waveguides has an exponential dependence on the refractive index of the surrounding analyte or cladding [Ebeling, 2003]. So, if the analyte can infiltrate the region between the coupled waveguides then the device can exploit this exponential dependence. This important observation has only been acknowledged and exploited in the literature once [Town et al., 2005]. The MCDC with its multiple coupled waveguides provides an ideal structure to investigate this exponential dependence.

The research presented in this thesis explores this exponential dependence of coupling with the analysis and design of MCDC structures for potential applications in sensing and electro-optic devices for integrated optics. The initial focus of the research was directed towards applications in sensing. It is shown that the application of the MCDC structure for evanescent field sensing provides a simpler and more robust interferometric sensing platform than a Mach-Zehnder interferometer. Sensors can be designed to provide high sensitivity and/or large dynamic range in a single device;

and the quasi-periodic dependence of coupling on analyte refractive index allows the sensor performance to be tuned by selecting an appropriate device length to fix the operating point at a corresponding sensitivity. Furthermore, a potential application in fluorescence sensing is explored with the design of a compact 1×2 WDM as a 'front end' for a fluorescence sensing system to facilitate a robust, portable and integratable, e.g. in a 'lab on a chip'.

Additionally, it was quickly realised that the use of recent electro-optic materials and the MCDC structure with its potential large bandwidth and simplicity of structure offered a significant alternative to the commonly used Mach-Zehnder interferometer, to allow the design of low cost, high speed electro-optic devices.

1.1.4 Electro-optic Effect

The electro-optic effect is a change in the optical properties of a material (refractive index or absorption) in response to an electric field that varies slowly compared with the frequency of light.

1.1.4.1 Pockels Effect

In certain types of materials, the application of an electric field results in a change in the material's refractive index that is linearly proportional to the applied electric field. This is known as the linear electro-optic effect, or Pockels effect, named after Friedrich Carl Alwin Pockels who discovered the effect in 1893.

The linear electro-optic effect is a second order non-linear optical process that requires

the electro-optic material to exhibit non-centrosymmetry, i.e. it does not possess inversion symmetry. Since the Pockels effect exists only in non-centrosymmetric materials it is often found in crystals such as lithium niobate where the crystalline structure provides long range symmetry and the non-centrosymmetry structure succumbs to asymmetric deformation under electric-field induced stress on the molecular structure. Other crystals and materials such as electric-field poled polymers also exhibit non-centrosymmetry and likewise produce a significant electro-optic response. In polymers, the alignment of chromophores with large hyperpolarisabilities can produce electro-optic effects that are over three times greater than found in the electro-optic crystal lithium niobate. This alignment is induced by heating the host polymer to its glass transition temperature and applying a large electric-field in order to orient the chromophores along the direction of the field. Chromophore alignment is retained by reducing the temperature of the host polymer under the continued electric field.

1.1.5 Electro-optic Materials

In this section, the recently discovered electro-optic crystal OH1 [Hunziker et al., 2008b] and the recently developed electro-optic polymer CLD-1/APC [Zhang et al., 2001] are discussed in relation to one of the most commonly used electro-optic materials, lithium niobate. It is shown that these recent alternate electro-optic materials offer significant advantages over lithium niobate in terms of larger electro-optic coefficients, relatively low dielectric constants and small dispersion in the index of refraction from dc to optical frequencies. This allows the design of low cost, high speed electro-optic devices using the MCDC structure with simple electrode structures that can be velocity and impedance matched.

1.1.5.1 Electro-optic Crystals

The electro-optic properties of crystals are due to a nonuniform redistribution of charges within the crystal lattice in the presence of an applied electric field [Yariv and Yeh, 2007]. This redistribution of charges causes slight deformations in the crystal lattice structure, which results in changes to the optical dielectric tensor.

The advantages of using crystals as the electro-optic material are that they offer superior thermal, orientational and photochemical stability compared with poled polymers [Jazbinšek et al., 2008]. Furthermore, crystals can be cut to any desired orientation to allow electric field orientation in any axis. The disadvantage is the relatively lower electro-optic coefficients compared to polymers.

There are several commercially available crystals that exhibit electro-optic properties. In this work, we shall consider two of these, lithium niobate and OH1.

1.1.5.1.1 Lithium Niobate

Lithium niobate is an inorganic crystalline electro-optic material with rhombohedral (trigonal) $3m$ symmetry. It is a uniaxial crystal, i.e. only one axis of the crystal called the optical axis allows an optical wave to propagate with an index of refraction that is independent of its polarisation direction. Thus $n_x = n_y \neq n_z$. It is customary to assign $\hat{z}$ to this axis.

Lithium niobate's three principal indices of refraction, can be described by one distinctive principal index of refraction called the extraordinary index n_e which coincides with the optical axis of the crystal, and two identical indices of refraction called the

ordinary index n_o. Thus $n_x = n_y = n_o$ and $n_z = n_e$. Furthermore, lithium niobate is a negative uniaxial crystal, where $n_e < n_o$.

Due to the trigonal $3m$ symmetry of the crystal, the electro-optic tensor has eight non-vanishing elements with four independent values: $r_{13} = r_{23}$, $r_{12} = r_{61} = -r_{22}$, r_{33}, and $r_{42} = r_{51}$; and takes on the form

$$r = \begin{bmatrix} 0 & -r_{32} & r_{13} \\ 0 & r_{22} & r_{13} \\ 0 & 0 & r_{33} \\ 0 & r_{42} & 0 \\ r_{42} & 0 & 0 \\ -r_{22} & 0 & 0 \end{bmatrix}. \tag{1.8}$$

The electro-optic coefficients of lithium niobate at 1550 nm are: $r_{22} = 8.6$ pm/V, $r_{13} = 3.4$ pm/V, $r_{51} = 28$ pm/V, and $r_{33} = 30.8$ pm/V [Turner, 1966]. The dielectric constants at infra-red wavelengths are $\epsilon_{11} = 41.5$ and $\epsilon_{33} = 44$ [Barker and Loudon, 1967]. The optical absorption characteristics measured for the bulk crystal have been found to be approximately 0.2 dB/cm for measurements in the visible and near infra-red spectral range [Wong, 2002].

Lithium niobate is one of the most commonly used electro-optic materials and is the most widely used electro-optic active substrate. Most commercial electro-optic devices are made from inorganic materials such as lithium niobate. Nevertheless, for some time now there has been great interest in electro-optic dielectric materials that provide an alternative to lithium niobate. This interest has been driven by the fact that lithium niobate's high dielectric constant limits device bandwidths to approximately 40 GHz.

So it has reached its practical limit in terms of very high speed applications, which require bandwidths well above 40 GHz.

1.1.5.1.2 OH1

The organic nonionic molecular crystal OH1 (2-(3-(4-Hydroxystyryl)-5,5-dimethylcyclohex-2-enylidene)malononitrile) is a novel nonlinear electro-optical crystal, with orthorhombic symmetry (point group $mm2$) [Hunziker et al., 2008b]; see Fig. 1.4. OH1 is a biaxial crystal, i.e. it has three distinct principal indices of refraction, with two optical axes, neither of which coincides with any one of the principal axes. Thus $n_x \neq n_y \neq n_z$.

The OH1 molecule and its crystal structure were first reported by Lemke [Lemke, 1970] and Kolev et al. [Kolev et al., 2001]. However, the potential of the OH1 molecule for applications in electro-optics has only recently been discovered [Brunner et al., 2008; Hunziker et al., 2008b; Kwon et al., 2008].

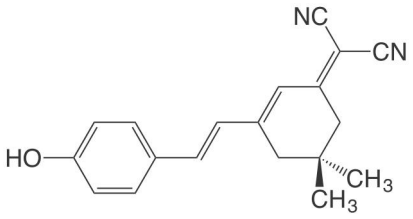

Figure 1.4: *Chemical structure of OH1*

OH1 crystals show a low absorption < 0.3 mm^{-1} over a large wavelength range between 680 and 1460 nm [Hunziker et al., 2009]. Single crystalline thin films with a very large area of more than 2 cm^2 and thickness between 0.1-4 μm have been fabricated on amorphous substrates, including glass and silicon-on-insulator [Hunziker et al.,

2008b]. These films exhibited very large electro-optic coefficients, e.g. r_{33} = 104 pm/V at 633 nm and r_{33} = 52 pm/V at 1319 nm, leading to very large electro-optic figures of merit of more than 500 pm/V in the whole transparency range [Hunziker et al., 2009].

Due to the orthorhombic $mm2$ symmetry of the crystal, the electro-optic tensor has five nonvanishing elements and independent values: r_{13}, r_{23}, r_{33}, r_{42}, and r_{51}; and takes on the form

$$r = \begin{bmatrix} 0 & 0 & r_{13} \\ 0 & 0 & r_{23} \\ 0 & 0 & r_{33} \\ 0 & r_{42} & 0 \\ r_{51} & 0 & 0 \\ 0 & 0 & 0 \end{bmatrix} \tag{1.9}$$

1.1.5.2 Electro-optic Polymers

Second-order nonlinear optical polymers (electro-optic polymers) have been intensively investigated in recent years as an alternative to lithium niobate. This has been due to their high electro-optic coefficients, ultrafast response times, low dielectric constants/losses, low material dispersion from dc to optical frequencies, relatively low cost and straightforward processing.

Organic electro-optic materials consist of many nonlinear optically active molecular units (chromophores) combined to create a bulk material. Chromophores are materials with extended π-electron conjugation in which the delocalized electron density

may be polarized easily in response to an applied electric field [Dalton et al., 2010]. These chromophores may be dispersed throughout an optically inactive (transparent) matrix such as a polymer. For use in practical devices, nonlinear optical chromophores must possess large molecular nonlinearity. Nonlinear optical properties occur from molecular level polarization of molecules of materials. In general, for large nonlinear optical properties, a nonlinear optical chromophore that possesses a large first hyperpolarizability is essential.

Several architectural classes for nonlinear optical polymers have been developed in the past decade, such as:

1. synthesizing highly efficient, chemically and thermally stable chromophores;
2. incorporating chromophores into material matrices;
3. chemical bonding the chromophores to the polymetric backbone (side-chain polymers);
4. blending physically (guest-host systems);
5. enhancing the extend of the interaction between polymer chains (cross-linked systems); and
6. incorporating inorganic glasses host materials (sol-gel systems).

The advantages of an electro-optic polymer include the large electro-optic coefficients and the relatively low dielectric constants. The disadvantages include thermal expansion, thermo-optic dependence and the restriction on the direction of the electro-optic axis from the limitation of poling normal to the surface of the polymer.

Significant research has been undertaken for guest-host non-linear electro-optic systems. The host polymer offers the main structure of the material while guest nonlinear chromophores induce the electro-optic sensitivity. Guest-host non-linear systems are acquired by doping the nonlinear chromophores into the polymer matrices via a subsequent electric field poling process. Thus, before the material can exhibit electro-optic qualities, it must first be poled to align the polarized nonlinear chromophore molecules distributed within the host polymer matrix to form an electro-optic axis. Once aligned, the presence of the electric field results in the chromophores producing a directional stress on the host polymer, effectively changing its optical properties.

1.1.5.2.1 CLD-1/APC

Recently, a highly active nonlinear chromophore CLD-1 was synthesised by Zhang et al. [2001]. CLD-1 is a ring-locked, phenyltetraene-based, second-order nonlinear optical chromophore. The chemical structure of CLD-1 is illustrated in Fig. 1.5. It is dispersed in an amorphous polycarbonate (APC) host polymer to form the guest-host system, CLD-1/APC. CLD-1 has also been dispersed in the host polymer Poly(methyl methacrylate) (PMMA) to form CLD-1/PMMA. However, PMMA is a relatively soft host polymer, which allows the chromophore orientation to relax over time due to its low glass transition (T_g = 100° C).

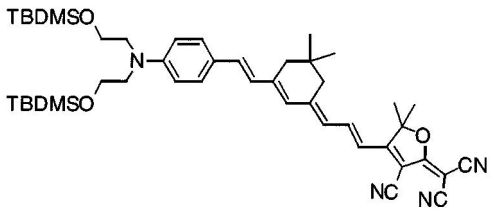

Figure 1.5: *Chemical structure of CLD-1*

An average electro-optic coefficient of 92 pm/V at 1060 nm has been achieved in a 25 wt % CLD-1/APC composite [Zhang et al., 2001]. The optical loss measured in CLD-1/APC thin-film slab waveguides was 1.2 dB/cm [Zhang et al., 2001]. Various devices have already been fabricated using CLD-1/APC including micro-ring resonators and Mach-Zehnder modulators [Poon et al., 2004; Zhang et al., 2001].

After poling, the electro-optic guest/host polymer's electro-optic tensor takes on the form

$$r = \begin{bmatrix} 0 & 0 & r_{13} \\ 0 & 0 & r_{13} \\ 0 & 0 & r_{33} \\ 0 & r_{13} & 0 \\ r_{13} & 0 & 0 \\ 0 & 0 & 0 \end{bmatrix} \tag{1.10}$$

where the z-direction is assumed as the direction of poling (electro-optic axis of the polymer).

1.1.5.3 Electro-optic Devices

Both the recently discovered electro-optic crystal OH1 and the recently developed electro-optic polymer CLD-1/APC offer the availability of an electro-optic material with large electro-optic coefficients, low dielectric constants and small dispersion in the index of refraction from dc to optical frequencies. This allows the potential design of low cost, high speed electro-optic devices, such as electro-optic switches and modulators with simple microstrip electrode structures that are velocity and impedance

matched.

The MCDC is an attractive structure for these sort of electro-optic applications because of its inherent large optical bandwidth and the simplicity of its structure. This is explored in the thesis with potential applications of the MCDC structure using these electro-optic materials for electro-optic devices, i.e. optical electric field sensors, switches and modulators.

1.2 Aims and Scope

The specific aims of the research reported in this thesis were to:

- investigate the MCDC structure for applications in sensing and switching;
- identify any possible advantages or limitations of the structure, and determine whether these could be exploited?
- investigate how best to utilise the exponential dependence of the coupling on the refractive index of the spacing material between the waveguides;
- investigate whether the sensitivity of a MCDC can be enhanced in any way?

The scope of this thesis is primarily limited to the analysis and design of planar waveguide MCDC structures. However, two publications are included in Chapter 3 where the MCDC structure is applied to optical fibers in the form of microstructured waveguide couplers for optical sensing.

1.3 Research Contributions

The research presented in this thesis makes the following contributions to the knowledge and understanding of the field:

- the identification and analysis of the phenomenon of partial image revivals in terms of the theory of supermodes [McCosker and Town, 2010i];
- exploitation of the phenomenon of partial image revivals to design a compact WDM for fluorescence sensing [McCosker and Town, 2010f];
- the design of a novel evanescent field optical sensor using the MCDC structure and polymer planar waveguides [McCosker and Town, 2010e];
- the design of a novel optical chemical sensor using the MCDC structure and silicon slot waveguides [McCosker and Town, 2010b];
- the discovery of the differential multi-channel directional coupler (DMCDC) structure and its use as an efficient optical chemical sensor using silicon slot waveguides [McCosker and Town, 2010g];
- the design of an all-dielectric optical electric field sensor based on a MCDC structure [McCosker and Town, 2010h];
- the design of a delta-κ electro-optic switch using the MCDC structure and the recently discovered electro-optic crystal OH1 [McCosker and Town, 2010d];
- the investigation and design of electro-optic modulators based on the MCDC structure using the recently developed electro-optic polymer CLD-1/APC and the electro-optic crystal OH1 [McCosker and Town, 2010d,c,a]

1.4 Thesis Outline

This is a thesis by publication, which is structured into 5 chapters. Chapters 2, 3 and 4 consist of a series of publications, which are preceded with an introduction that provides the context of the publications in terms of how they fit into the overall thesis. Following Macquarie University's guidelines for a thesis by publication, each publication is presented as it has been printed (published), or in the case of manuscripts still under review, in the format they were submitted.

Chapter 1 introduces the MCDC structure and provides background to the work contained in the thesis. It details the aims, scope and research contributions of the thesis.

Chapter 2 presents the analysis and design of MCDC structures. It consists of two publications. The first publication identifies a potential limitation of the MCDC with the discovery and subsequent analysis of the phenomenon of partial image revivals [McCosker and Town, 2010i]. The second publication describes the exploitation of the phenomenon of partial image revivals to design a compact WDM for fluorescence sensing using a MCDC structure [McCosker and Town, 2010f]. The WDM is designed to be a 'front-end' for a compact fluorescence sensing system that is integratable, e.g. in a 'lab-on-a-chip'.

Chapter 3 presents applications of the MCDC structure in optical evanescent field sensing. It consists of five publications. The first publication describes an evanescent field optical sensor using the MCDC structure and polymer planar waveguides [McCosker and Town, 2010e]. If the analyte infiltrates the spacing between the coupled waveguides then the sensor can exploit the exponential dependence of the coupling

on the analyte refractive index for sensitivity and dynamic range. The second publication describes an optical chemical sensor using the MCDC structure with silicon slot waveguides [McCosker and Town, 2010b]. If the analyte infiltrates both the spacing between the coupled waveguides and the slots in the waveguides themselves then the sensor can exploit the high confinement of light in the slots to enhance the overall sensitivity of the sensor whilst retaining the exponential dependence of the coupling on the analyte refractive index. The third publication describes an optical chemical sensor using a differential multi-channel directional coupler structure with slot waveguides [McCosker and Town, 2010g]. The differential nature of the structure provides a more efficient sensor, i.e. higher sensitivity and shorter device length. The fourth publication provides an overview of microstructured waveguide devices for applications in optical sensing, i.e. the design of arrays of coupled waveguides in either planar or fiber for which the transmittance is highly sensitive to the refractive index of the material in the slots or holes [Town et al., 2010a]. The final publication describes an equivalent MCDC structure in a non-planar waveguide form for refractive index sensing of an analyte, i.e. dual-core microstructured optical fiber [Town et al., 2010b].

Chapter 4 explores the use of recent electro-optic materials in a MCDC for application as electro-optic devices. It consists of four publications. The first publication describes an optical electric field sensor using the MCDC structure [McCosker and Town, 2010h]. The second publication describes an electro-optic switch using the MCDC structure incorporating the recently discovered electro-optic crystal OH1 for the cladding layer [McCosker and Town, 2010d]. The third publication describes a delta-κ electro-optic modulator using a MCDC incorporating the recently developed electro-optic polymer CLD-1/APC for the cladding layer [McCosker and Town, 2010c]. The final publication describes a delta-β electro-optic modulator incorporating the

electro-optic polymer CLD-1/APC for the waveguide cores and analyses the various optimisations possible [McCosker and Town, 2010a].

Chapter 5 concludes the thesis by providing a synthesis of the work described in the proceeding chapters; and summarises the research contributions to the knowledge and understanding in the field. Ideas for further research are also presented.

Finally, an appendix is included that provides background electro-optic theory, which was considered assumed knowledge in the publications of Chapter 4.

How poor are they that have not patience!
What wound did ever heal but by degrees?
Thou know'st we work by wit, and not by witchcraft;
And wit depends on dilatory time.

William Shakespeare,
Iago, *Othello* (2.3.376-379)

2

Analysis and Design

2.1 Introduction

In this chapter, the multi-channel directional coupler (MCDC) is analysed using the theory of supermodes [Yariv, 1997] to identify any inherent limitations that may affect the design of MCDC devices; and subsequently a compact WDM is designed using the results of the analysis.

This chapter represents the initial stage of the research, the goal of which was to determine whether the length of a MCDC could be decreased to form more compact devices by simply increasing the coupling. During this stage the phenomenon of partial image revivals was identified and analysed. The resulting work is presented as the first pub-

lication of this chapter: *"Partial Image Revivals in a Multi-Channel Directional Coupler"* [McCosker and Town, 2010i] . Subsequently, we realised that it was possible to take advantage of this phenomenon to design more compact MCDC devices. This allowed us to exploit the MCDC structure for both its inherent large bandwidth (that scales with device length) while maintaining a compact design. Consequently, we designed a compact 1×2 WDM as a 'front end' for a fluorescence sensing system to facilitate a robust, portable and integratable, e.g. in a 'lab on a chip'; which is able to be fabricated in low cost polymer. The resulting work is presented as the final publication of this chapter: *"Multi-Channel Directional Coupler for WDM in Fluorescence Sensing"* [McCosker and Town, 2010f].

2.2 Publications

The remaining chapter consists of the following two publications:

1. Ravi J. McCosker and Graham E. Town, **Partial Image Revivals in a Multi-Channel Directional-Coupler**, in *Proceedings of the SPIE*, 2010, vol. 7604, pp. 76040G 1-10.

2. Ravi J. McCosker and Graham E. Town, **Multi-Channel Directional Coupler for WDM in Fluorescence Sensing**, submitted to *IEEE Journal of Lightwave Technology*.

, . ., & To , . . (201). - -
p . *r* *ng* *h* , 4, p. 4 -1- 4 -1 .

DOI: 10.1 7/ 2. 4 2

Multi-Channel Directional Coupler for WDM in fluorescence sensing

Ravi J. McCosker, *Student Member, IEEE,* and Graham Town, *Senior Member, IEEE.*

***Abstract*—We describe a 1×2 WDM for fluorescence sensing using a multi-channel directional coupler structure. The WDM is designed to be a 'front end' for a compact fluorescence sensing system that is integratable e.g. in a 'lab-on-chip'.**

***Index Terms*—Multi-channel directional coupler (MCDC), fluorescence sensing, Wavelength division multiplexing (WDM).**

I. Introduction

One of the key driving forces behind the demand for optical sensors has been from the healthcare and biotechnology industry which require compact devices offering generic sensing strategies at low cost and suitable for application in portable instrumentation [1]. Fluorescence-based detection systems have attracted attention because of their potential to provide both high sensitivity and specificity. However, with a few recent exceptions [2], [3] fluorescence-based detection systems have typically been expensive and non-compact. As a result the integration of fluorescence detection systems as a 'lab-on-a-chip' system has received considerable attention [4].

II. Theory

A. Multi-Channel Directional Coupler

The multi-channel directional coupler (MCDC) [5] consists of an array of identical and equally spaced channel waveguides buried in a cladding layer (Fig. 1). The waveguides are in sufficiently close proximity that they may be considered to be a coupled system rather than an array of individual waveguides. Incident light focused into the input or feed waveguide will couple into the adjacent waveguides.

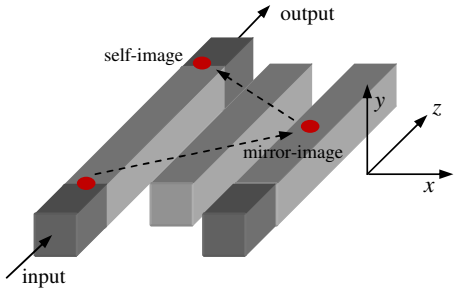

Fig. 1. Schematic of a side-fed 3-channel multi-channel directional coupler with single input and output ports indicated. Mirror- and self-images of the input field are also indicated.

Ravi J. McCosker is with the Department of Electronic Engineering, Macquarie Unviersity, NSW 2109, Australia email: ravi.mccosker@mq.edu.au

November 29, 2010

B. Supermodes

Using the theory of supermodes [6], the MCDC can be described as a single composite waveguide structure that support multiple modes or supermodes [7]. Supermodes are eigenmodes of coupled (waveguide) systems. They may be derived by diagonalisation of the matrix describing the coupling between the unperturbed modes of the individual waveguides. A system of N weakly coupled waveguides can be regarded as supporting N supermodes, each with a constant amplitude and unique propagation constant. Together the supermodes beat to form a multi-mode interference (MMI) pattern along the direction of propagation of the device. As a result, the input field is revived or imaged at periodic intervals along the device. The operation of the MCDC can then be analysed in terms of MMI for periodic imaging [8].

C. Adjacent Waveguide Coupling

A 3-channel MCDC (Fig. 1) supports three supermodes and the side-fed configuration excites all three of them. If the waveguides are far enough apart that non-adjacent waveguide coupling can be ignored then the supermode propagation constants σ are given by [7]

$$\begin{aligned} \sigma_1 &= \beta + \sqrt{2}\kappa \\ \sigma_2 &= \beta \\ \sigma_3 &= \beta - \sqrt{2}\kappa \ , \end{aligned} \tag{1}$$

where β denotes the propagation constant common to each unperturbed waveguide; κ is the common coupling coefficient; and σ_1 is the fundamental supermode propagation constant.

For a specified wavelength the image length for a 3-channel MCDC can be written in terms of the supermode spacings as [9]

$$L = i\frac{v\pi}{\sigma_1 - \sigma_v} \ ; \qquad v = 2, 3; \ i > 0 \ , \tag{2}$$

where σ_v is the v_{th} supermode propagation constant, and the parity of i denotes whether the image formed is either a mirror-image (odd) or a self-image (even). Alternatively, by substituting (1) into (2) the image lengths can be written in terms of the coupling coefficient as

$$L = i\frac{\pi}{\sqrt{2}\kappa} \qquad i > 0 \ . \tag{3}$$

Examination of (3) indicates that in order to reduce the image length of the device, the coupling coefficient needs to be increased, for example, by decreasing the spacing between each waveguide.

D. Non-Adjacent Waveguide Coupling

If the waveguides are in sufficiently close proximity then both adjacent waveguide coupling denoted by the coupling coefficient κ_1 and non-adjacent waveguide coupling denoted by the coupling coefficient κ_2 must be considered. In this case, the supermode propagation constants σ are given by [9]

$$\begin{aligned}\sigma_1 &= \beta + \tfrac{1}{2}\left(\kappa_2 + \sqrt{\kappa_2^2 + 8\kappa_1^2}\right)\\ \sigma_2 &= \beta - \kappa_2\\ \sigma_3 &= \beta + \tfrac{1}{2}\left(\kappa_2 - \sqrt{\kappa_2^2 + 8\kappa_1^2}\right)\ .\end{aligned} \tag{4}$$

Subsequently, we can derive the supermode propagation spacings as

$$\begin{aligned}\sigma_1 - \sigma_2 &= \tfrac{1}{2}\left(3k_2 + \sqrt{k_2^2 + 8k_1^2}\right)\\ \sigma_1 - \sigma_3 &= \sqrt{k_2^2 + 8k_1^2}\ .\end{aligned} \tag{5}$$

For a 3-channel MCDC, the mirror-image length can be written in terms of the supermode propagation spacings as [9]

$$L = m\frac{\pi}{\sigma_1 - \sigma_2} = n\frac{2\pi}{\sigma_1 - \sigma_3}\ , \tag{6}$$

where *m* is odd; and the self-image length is simply twice that of the mirror-image. Rearranging (5) gives the second supermode propagation spacing as

$$\sigma_1 - \sigma_2 = \frac{1}{2}\left[(\sigma_1 - \sigma_3) + 3k_2\right]\ , \tag{7}$$

which can then be substituted into (6) to give

$$L = m\frac{\pi}{(\sigma_1 - \sigma_3) + 3k_2} = n\frac{\pi}{\sigma_1 - \sigma_3}\ , \tag{8}$$

where *m* and *n* are integers. In this case, the image length is written in terms of the second supermode propagation spacing $\sigma_1 - \sigma_3$ and shows a weak perturbation or shift by the presence of the non-adjacent coupling κ_2. This indicates that as the supermodes propagate along the device, they slowly drift in and out of phase forming a more complex interference pattern due to this weak perturbation. The result is the formation of what we refer to as partial images at periodic intervals along the direction of propagation of the device [9].

Referring to (8) and considering that the supermode propagation spacing is much larger than the coupler coefficient κ_2, that is $(\sigma_1 - \sigma_3) \gg \kappa_2$ then for a 3-channel MCDC we can describe the partial image points by

$$L_{partial-image} \approx i\frac{2\pi}{\sigma_1 - \sigma_3}\ ; \qquad i > 0\ , \tag{9}$$

where the parity of *i* denotes whether the partial image formed is either a mirror-image (odd) or a self-image (even). We can take advantage of the partial images that occur near complete images as they are themselves almost complete images.

E. WDM

A device can separate two wavelengths λ_1 and λ_2 if it acts as a bar-coupler (self-image) for one wavelength and a cross-coupler (mirror-image) for the other wavelength. Accordingly, the device length is given by [8]

$$L_{\text{mcdc}} = pL_{\lambda_1} = (p+q)\,L_{\lambda_2}\ , \tag{10}$$

where p is a natural number, q is an odd integer, and L_{λ_1} and L_{λ_2} are the associated partial image lengths for the wavelengths λ_1 and λ_2, respectively.

For the appropriate length calculated from Eq. (10) the device forms a self-image at wavelength λ_1 and hence extending the left outside waveguide beyond the MCDC section (Fig. 1), forms a bar-coupled output waveguide. Alternatively, the device forms a mirror-image at wavelength λ_2 and hence extending the right outside waveguide beyond the MCDC section (Fig. 1), forms a cross-coupled output waveguide.

III. Design

For the purposes of illustrating device performance in this work, the fluorophore is assumed to be Dylight 680 (Thermo Scientific), with an excitation and emission maxima at 692 nm and 712 nm, respectively. The system could then use a 692 nm LED source for excitation of the fluorophore with a corresponding spectra FWHM of around 10-15 nm.

The design is reciprocal in that two separate filter responses are calculated independently. Firstly, we designed the pump to fluorophore path i.e. the MCDC initially provides a cross-coupled path for the pump (excitation source) to the fluorophore (Fig. 2). Next, we designed the fuorophore to detector path that operates in the opposite direction i.e. the MCDC removes the excitation light from the resulting fluorescence spectra. It does this by performing a demultiplexer operation, where the excited 712 nm light is bar-coupled to the output detector (Fig. 2).

Fig. 2. Schematic of MCDC device.

We selected a 3-channel MCDC for a compact device structure. This configuration offers the best performance in terms of sensitivity and bandwidth when compared to other possible configurations [10]. A cross section of the device is shown in Fig. 3.

The device is composed of identical channel waveguides of cross section 800×800 nm (w×h) for single mode operation over both wavelengths. The gap between each waveguide is s = 520 nm. This is the closest we can make the waveguides for a compact design that provides an aligned output for

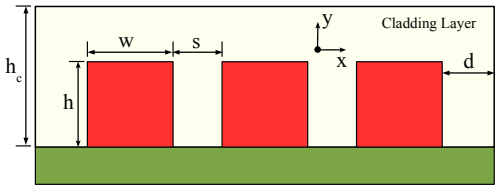

Fig. 3. Schematic of 3-channel multi-channel directional coupler WDM.

both wavelengths. We assumed the channel waveguides to be composed of the polymer SU-8, with a refractive index of 1.58 at 692 nm. The waveguides are buried in a cladding layer of height $h_c = 2$ μm. The device sites on a glass substrate with refractive index of 1.44.

IV. Results and Discussion

The transfer characteristics of the MCDC were determined using an Eigen-Mode Propagation technique [11] implemented with COMSOL and MATLAB. The simulated power evolution along the MCDC for the reciprocal design (692/712 nm) is shown in Fig 4. The design uses a partial self-image point to extract the 692 nm pump to the fluorophore/analyte, and a complete mirror-image point to extract the 712 nm excitation signal to the detector.

The aim is to collect as much signal as possible, while filtering out as much pump and other noise as possible. The key WDM filter performance parameters are: isolation between the source and detector channel; bandwidth (especially of detector channel); and insertion loss (especially of detector channel). The isolation ratio (IR) and insertion loss (IL) in decibels, are defined as

$$\mathrm{IR} = 10\log\left(\frac{P_{\mathrm{out}}}{P_{\mathrm{outW}}}\right) \;; \qquad \mathrm{IL} = -10\log\left(\frac{P_{\mathrm{out}}}{P_{\mathrm{in}}}\right) , \qquad (11)$$

where P_{out} and P_{outW} denote the fractional powers in the right and wrong output ports, respectively; and P_{in} denotes the power to the input port.

The simulated isolation ratio and insertion loss as a function of wavelength variation are shown in Fig. 5. Isolation ratios of 20/44 dB and insertion losses of 0.3/0.1 dB at 692/712 nm, respectively are predicted. In addition, 3-dB bandwidth were measured in terms of the isolation ratio as 12/18 nm for 692/712 nm, respectively. The design results in a trade-off between device length and isolation ratio. Although we used

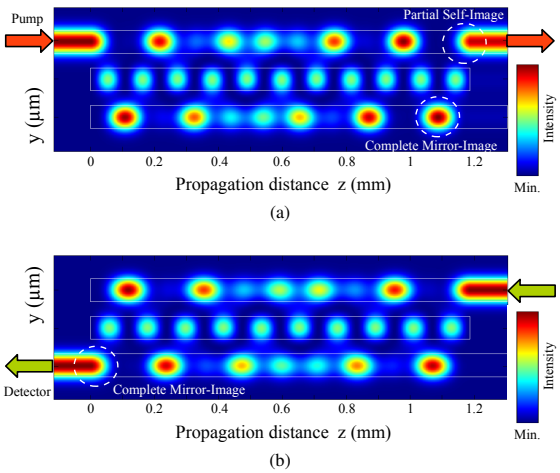

Fig. 4. Simulated power evolution along the MCDC for (a) pump (692 nm) is input at left-side input and extracted at right-side output for fluorophore excitation; output is at a partial self-image; (b) excited fluorescence signal (712 nm) is input at right-side input and extract at left-side output for detection; output is at a complete mirror-image.

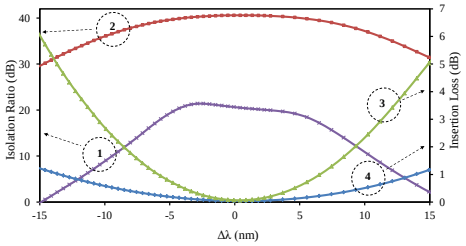

Fig. 5. Simulated device performance against wavelength (λ): (1) Isolation ratio for 692 nm; (2) Isolation ratio for 712 nm; (3) Insertion loss for 692 nm; (3) Insertion loss for 712 nm.

a partial self-image to extract the 692 nm pump to the fluorophore/analyte, this resulted in a reduced isolation ratio when compared to the extraction of the 712 nm excitation signal to the detector, which uses a complete mirror-image. Furthermore, we note that the 712 nm spectra exhibits a flatter, non-sinusoid response. This is a result of the presence of the partial image and therefore the influence of non-adjacent waveguide coupling on the response.

V. Conclusion

We described a 1×2 WDM for fluorescence sensing using a 3-channel MCDC structure. The entire device has a footprint of 3.44×2.8×1190 μm (w×h×L). Numerical simulations demonstrate insertion losses of 0.3/0.01 dB, isolation ratios of 20/44 dB and 3-dB bandwidths of 12/18 nm for 692/712 nm, respectively.

References

[1] A. P. Demchenko, *Introduction to fluorescence sensing*. Springer, 2008.

[2] A. Cleary, S. Garcia-Blanco, A. Glidle, J. Aitchison, P. Laybourn, and J. Cooper, "An integrated fluorescence array as a platform for lab-on-a-chip technology using multimode interference splitters," *IEEE Sensors J.*, vol. 5, pp. 1315–1320, 2005.

[3] E. Thrush, O. Levi, L. J. Cook, J. Deich, A. Kurtz, S. J. Smith, W. Moerner, and J. S. H. Jr., "Monolithically integrated semiconductor fluorescence sensor for microfluidic applications," *Sens. Actuators, B*, vol. 105, pp. 393–399, 2005.

[4] A. Manz, N. Graber, and H. M. Widmer, "Miniaturized total chemical-analysis systems: A novel concept for chemical sensing," *Sens. Actuators, B*, vol. 1, pp. 244–248, 1990.

[5] S. R. Somekh, "Theory, fabrication and performance of some integrated optical devices," Ph.D. dissertation, California Institute of Technology, California, 1974.

[6] A. Yariv, *Optical Electronics in Modern Communications*. Oxford Univ. Press, New York, 1997.

[7] E. Kapon, J. Katz, and A. Yariv, "Supermode analysis of phase-locked arrays of semiconductor lasers," *Opt. Lett.*, vol. 9, pp. 125–127, 1984.

[8] L. B. Soldano and E. C. M. Pennings, "Optical multi-mode interference devices based on self-imaging: Principles and applications," *J. Lightw. Technol.*, vol. 13, pp. 615–627, 1995.

[9] R. J. McCosker and G. E. Town, "Partial image revivals in a multi-channel directional-coupler," *Proc. SPIE*, vol. 7604, p. 76040G, 2010.

[10] R. J. McCosker and G. E. Town, "Multi-channel directional coupler as an evanescent field optical sensor," *Sensors and Actuators B*, vol. 150, pp. 417–424, 2010.

[11] D. F. G. Gallagher and T. P. Felici, "Eigenmode expansion methods for simulations of optical propagation in photonics - pros and cons," *Proc. SPIE*, vol. 4987, pp. 69–82, 2003.

Sometimes the situation is only a problem because it is looked at in a certain way. Looked at in another way, the right course of action may be so obvious that the problem no longer exists.

Edward de Bono

3

Optical Sensors

3.1 Introduction

This chapter presents potential applications of the multi-channel directional coupler (MCDC) structure for optical evanescent field sensing. This represents a continuation of my primary supervisor Professor Graham Town's original concept of using the MCDC as an optical evanescent field sensor [Town et al., 2005]. This concept involved the idea that if the analyte infiltrates the spacing between the coupled waveguides then the MCDC can exploit the exponential dependence of the coupling on the refractive index of the analyte [Ebeling, 2003]. Subsequent changes to the refractive index of the analyte will cause a shift in the image length, and therefore the power transmitted to

the output (waveguide) of the MCDC.

The first publication in this chapter, "*Multi-Channel Directional Coupler as an Evanescent Field Optical Sensor*" [McCosker and Town, 2010e] presents an analysis of the MCDC structure for evanescent field optical sensing using polymer planar waveguides. This work identifies the optimum configuration for sensitivity and dynamic range. It also considers the impact of partial image revivals (see Chapter 2) on sensor transmittance.

Following on from this publication, I considered the use of silicon slot waveguides to exploit the high confinement of light in the slot regions to increase the overall sensitivity of the sensor, whilst retaining the exponential dependence of the coupling on the analyte refractive index. The resulting work is presented as the second publication in this chapter: "*Optical Chemical Sensor using a Multi-Channel Directional Coupler with Slot Waveguides*" [McCosker and Town, 2010b].

From my work on chemical sensing and electro-optic modulation using the MCDC structure (see Chapter 4), I discovered the differential multi-channel directional coupler (DMCDC) structure. This structure represents the most efficient configuration for the MCDC, i.e. higher sensitivity and shorter device length. I applied the DMCDC structure to design a chemical sensor. The resulting work is presented as the third publication in this chapter: "*Optical Chemical Sensor using a Differential Multi-Channel Directional Coupler with Slot Waveguides*" [McCosker and Town, 2010g].

The fourth publication in this chapter "*Design of Microstructured Waveguide Devices for Applications in Optical Sensing*", [Town et al., 2010a] provides an overview of microstructured waveguide devices for applications in optical sensing, i.e. the design of

arrays of coupled waveguides in either planar or fiber for which the transmittance is highly sensitive to the refractive index of the material in the slots or holes.

The final publication in this chapter "*Microstructured Optical Fiber Refractive Index Sensor*" [Town et al., 2010b] describes an equivalent MCDC structure in a non-planar waveguide form for refractive index sensing of an analyte, i.e. dual-core microstructured optical fiber.

3.2 Publications

The remaining chapter consists of the following five publications:

1. Ravi J. McCosker and Graham E. Town, **Multi-Channel Directional Coupler as an Evanescent Field Optical Sensor**, *Sensors and Actuators B* 150 (2010), pp. 417-424.

2. Ravi J. McCosker and Graham E. Town, **Optical Chemical Sensor using a Multi-Channel Directional Coupler with Slot Waveguides**, in *Proceedings of the International Conference on Photonics (ICP)*, Langkawi, 2010, pp. 1-5.

3. Ravi J. McCosker and Graham E. Town, **Optical Chemical Sensor using a Differential Multi-Channel Directional Coupler with Slot Waveguides**, submitted to *Sensors and Actuators B*.

4. Graham E. Town, Ravi McCosker, Wu Yuan, and Ole Bang, **Design of Microstructured Waveguide Devices for Applications in Optical Sensing**, in *Proceedings of the Optics & Photonics Congress, Advanced Photonics & Renewable Energy*, Karlsruhe, 2010.

5. Graham E. Town, Wu Yuan, Ravi McCosker and Ole Bang, **Microstructured Optical Fiber Refractive Index Sensor**, *Optics Letters* 35 (2010), pp. 856-858.

, . ., & To , . . (201). - p
p . *n r an a r* , , p. 4 -424.

DOI: 10.10 / .s .2 . . 22

Erratum

The authors wish to provide a correction to a figure in the publication, "Multi-Channel Directional Coupler as an Evanescent Field Optical Sensor" in *Sensors and Actuators B* 150 (2010), pp. 417-424.

Figure 9(b) on page 421 incorrectly shows the modal power evolution of the input (upper) waveguide. The correct complete version of Figure 9 is:

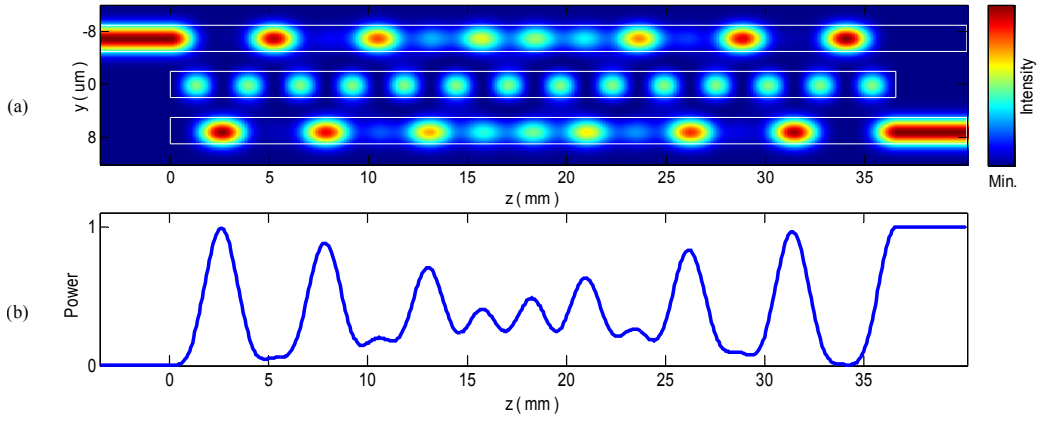

Fig 9: Simulated (a) field evolution along a side-fed 3-channel MCDC that shows a periodic partial image phenomenon; (b) modal power evolution of output (lower) waveguide.

, . ., & To , . . (201). p -
p . *r ng n rna na n r n n h n , , 2 - .*

DOI: 10.1 09/ .2 . 44 9

Optical Chemical Sensor using a Differential Multi-Channel Directional Coupler with Slot Waveguides

Ravi J. McCosker[a,*], Graham E. Town[a]

[a]*MQ Photonics Research Centre, Department of Electronic Engineering, Macquarie University, NSW 2109, Australia.*

Abstract

We describe a novel chemical sensor based on a differential multi-channel directional coupler structure with slot waveguides. The sensitivity of the sensor exploits the exponential dependence of the waveguide coupling on the analyte refractive index, the strong confinement of light in the slot waveguides, and the differential nature of the structure itself.

Keywords: Multi-channel directional coupler, Optical sensor, Evanescent field, Analyte, Supermode.

1. Introduction

Integrated optics has enabled the development of compact, high performance and low-cost chemical sensors [1]. Optical chemical sensors are used in applications such as, environmental monitoring, medicine, biomedicine and chemical analysis [2]. Various optical chemical sensor structures have been proposed, such as Mach-Zehnder interferometers [3], microring resonators [4], slot waveguides [5, 6], directional couplers [7, 8], multi-mode interference couplers [9], and multi-channel directional couplers [10, 11]. In these devices, homogeneous sensing is performed by the evanescent tail of the modal field in the cover medium. The sensing operation consists of measuring the change of the effective index of a propagating mode when a change in the external analyte refractive index takes place [12].

In a previous work [13] we described a chemical sensor based on a multi-channel directional coupler structure with slot waveguides. We showed that if the analyte infiltrates the slot region of the waveguides and the spacing between each waveguide then the sensitivity of the device can exploit both the strong confinement of light in the slot waveguides and the exponential dependence of the waveguide coupling on the analyte refractive index. In this work, we describe a more sensitive chemical sensor based on a differential multi-channel directional coupler structure where the centre slot region is filled with another material, preventing the centre slot region from being infiltrated by the analyte.

2. Slot waveguide

The slot waveguide is a high-index contrast photonic wire that has attracted significant research interest since its proposal by Almeida et al. in 2004 [14]. In conventional waveguides the majority of the optical power, including the peak intensity, is located in the high-index core. In contrast, a slot waveguide is able to confine and guide light in a nanometre sized low-index slot region. This characteristic makes the slot waveguide attractive for sensing applications. Using the slot region to probe the cover medium or analyte will result in a larger light/analyte interaction and hence higher sensitivity than conventional waveguide [5, 4, 6]

A slot waveguide consists of a sub-wavelength low-index slot region embedded between two rails of a high-index material, as shown in Fig. 1(a). For the polarisation mode where the orientation of the electric field is perpendicular to these high-index contrast interfaces, the electric field undergoes a large discontinuity at the boundaries, which results in a large fraction of the guided optical power to be strongly confined in the small slot region [14]. In the case of a vertical slot waveguide, the electric field of the quasi-TE eigenmode is strongly confined in the slot region, as shown in Fig. 1(b).

2.1. Sensitivity

A slot waveguide as an evanescent field sensor relies on an effective index change to the guiding structure as a result of a cover medium or analyte refractive index change [8].

In this work, the analyte is assumed to infiltrate into the slot region of the waveguide. We consider the analyte is constituted by an aqueous solution, such as deionised water, whose refractive index is dependent on the concentration of a chemical agent dispersed in the solution. Examples, of possible chemical agents and their ambient refractive indices in deionised water (n = 1.33) for 1550 nm are: glucose (n = 1.333), ethanol (n = 1.36), isopropanol (n = 1.37) and cycohexane (n = 1.42) [4]. We also note that biochemical components could also be used.

The waveguide sensitivity S_{slot} to an analyte refractive index n_a change can be defined as [12]

$$S_{\text{slot}} = \frac{\partial n_{\text{eff}}}{\partial n_a} , \quad (1)$$

*Tel: +612 9850 8439; Fax: +612 9850 9128.
Email address: ravi.mccosker@mq.edu.au (Ravi J. McCosker)

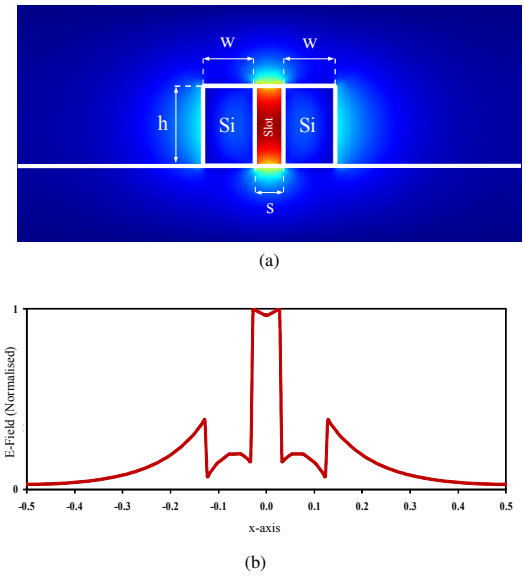

Figure 1: (a) Cross section of a vertical slot waveguide that consists of a low-index analyte slot region (n = 1.33), embedded between two Si rail waveguides (n = 3.476). The geometric parameters: rail width w, slot width s, and slot waveguide height h are indicated. The calculated Electric field E_x distribution of the quasi-TE eigenmode over the cross section for a wavelength of 1550 nm is also shown. (b) Electric field amplitude of the quasi-TE eigenmode across the centre of the waveguide. This shows the high electric field confinement in the low-index slot region.

where n_{eff} denotes the effective index of the slot waveguide eigenmode.

2.2. Design

In this work, we designed single-mode slot waveguides for 1550 nm. The rail regions were considered to be composed of Si with a refractive index n = 3.476. The slot waveguides were considered to be built on a silicon-on-insulator platform where the waveguides are located on top of a thick SiO_2 (n = 1.444) buffer layer and a Si substrate.

The slot waveguide sensitivity S_{slot} was optimised numerically while maintaining the single-mode condition by varying the slot waveguide geometric parameters: rail width w, slot width s, and slot waveguide height h; as indicated in Fig. 1(a). We used a 2-D full-vectorial Finite Element Method to numerically calculate the effective index n_{eff} for these geometric parameters and an analyte refractive index n_a range of 1.33 – 1.42.

The final optimised slot waveguide has a sensitivity S_{slot} = 0.976; with the following dimensions: w = 180 nm, s = 100 nm, and h = 300 nm.

3. Differential multi-channel directional coupler sensor

In this section, we describe a chemical sensor using a differential multi-channel directional coupler structure and the optimised slot waveguides from section 2. The analyte is assumed to surround the structure, and infiltrate the spacing between each waveguide and also the slot region of the outside waveguides of the sensor.

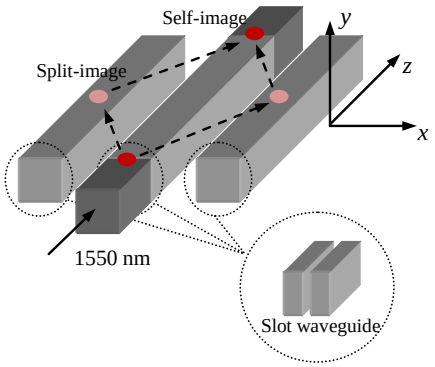

Figure 2: A schematic of a centre-fed 3-channel multi-channel directional coupler with slot waveguides. The input or centre-fed waveguide, a split-image and a self-image of the input field are also indicated.

3.1. Multi-channel directional coupler

A multi-channel directional coupler (MCDC) [15] consists of an array of identical and equally spaced waveguides (Fig. 2). The waveguides are in sufficiently close proximity that they may be considered to be a coupled system rather than an array of individual waveguides. Incident light focused into the input or feed waveguide will couple into the adjacent waveguides. In this work the waveguides are considered to be slot waveguides.

3.2. Differential Multi-Channel Directional Coupler

We define a differential multi-channel directional coupler (DMCDC) as a MCDC that consists of an odd number of waveguides, where all waveguides are equally spaced and identical except the centre waveguide.

In this work, we consider a centre-fed 3-channel DMCDC with slot waveguides where the slot region of the centre slot

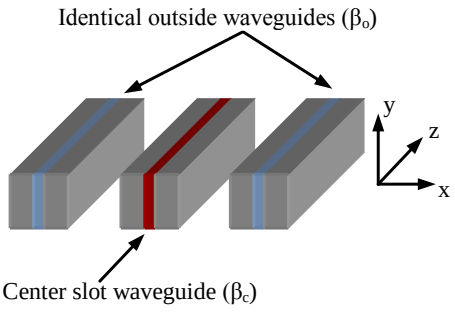

Figure 3: A schematic of a section of a 3-channel differential multi-channel directional coupler with slot waveguides. All three waveguides have identical dimensions. The outside slot waveguides are identical with an unperturbed propagation constant β_o. The centre slot waveguide has a different slot region material and hence a different unperturbed propagation constant β_c.

waveguide consists of a different material than the other outside slot waveguide regions (Fig. 3). All three waveguides have identical dimensions ($w \times h$). The identical outside slot waveguides have an unperturbed propagation constant β_o. However, the centre slot waveguide with a different slot material will therefore have a different unperturbed propagation constant β_c.

3.3. Supermodes

According to the theory of supermodes [16], the eigenmodes of a system consisting of an array of coupled waveguides can be obtained by a diagonalisation of the coupled-mode equations used to describe them. The electric field of these new modes or so-called supermodes is considered as a linear combination of the original modes of the separate (uncoupled) waveguides.

Using supermode theory, the MCDC can be modelled as a single composite waveguide structure that supports multiple supermodes [17]. Each supermode has a constant amplitude and unique propagation constant. Together, the supermodes beat to form a multi-mode interference (MMI) pattern along the direction of propagation of the device. As a result, the input field is revived or imaged at periodic intervals along the device [18]. The operation of the MCDC can then be analysed in terms of MMI for periodic imaging [19].

Consider a centre-fed 3-channel DMCDC that consists of an array of three slot waveguides. Each waveguide is presumed to support a single quasi-TE mode. This mode is described by its electric field $\varepsilon(x,y)\exp_n(-j\beta_n z)$ where β_n is the propagation constant of the n$^{\text{th}}$ waveguide. The electric field distribution E_y of the waveguide array can be approximated by the superposition of the decoupled waveguide modes [17] as

$$E_y = \hat{y}\sum_{n=1}^{3} A_n(z)\,\varepsilon(x,y)\exp(-j\beta_n z) \tag{2}$$

where $A_n(z)$ denote the waveguide complex amplitudes, and the z dependence is due to the interaction among the array waveguides. We can uniquely describe the field at z by means of a column vector

$$\boldsymbol{E}(z) = \begin{bmatrix} A_1(z)\exp(-j\beta_1 z) \\ A_2(z)\exp(-j\beta_2 z) \\ A_3(z)\exp(-j\beta_3 z) \end{bmatrix} = \begin{bmatrix} E_1(z) \\ E_2(z) \\ E_3(z) \end{bmatrix} \tag{3}$$

The evolution of $\boldsymbol{E}(Z)$ is obtained from the coupled mode equations as

$$\frac{d\boldsymbol{E}}{dz} = -jM\boldsymbol{E} \tag{4}$$

where M denotes the coupling matrix.

Assuming only adjacent waveguide coupling and the 3-channel DMCDC structure discussed in section 3.2 where $\beta_o = \beta_1 = \beta_3$ and $\beta_c = \beta_2$ (Fig. 3) then the coupling matrix is given by

$$M = \begin{bmatrix} \beta_o & \kappa & 0 \\ \kappa & \beta_c & \kappa \\ 0 & \kappa & \beta_o \end{bmatrix} \tag{5}$$

where κ is the coupling coefficient for the adjacent waveguides.

Considering the eigenmodes of M are z dependent only by a propagation phase factor, we can assume the eigensolutions are the eigenvectors that satisfy

$$E_v(z) = E_v(0)\exp(-j\,\sigma_v\,z)\ . \tag{6}$$

Combining (4) and (6) results in the eigenmode problem

$$M\boldsymbol{E} = -j\sigma\boldsymbol{E} \tag{7}$$

for which the supermodes of the array are defined as its eigensolutions; $\boldsymbol{E}$ is the eigenvector and $-j\sigma$ is the eigenvalue of M, where σ denote the supermode propagation constants.

Although the 3-channel DMCDC supports three supermodes, the centre-fed configuration only excites the two odd symmetric supermodes (Fig. 4). The excited supermodes have the eigenvectors

$$E_{1,3} = \frac{1}{\sqrt{2}}\begin{pmatrix} 2\kappa/\left(-\delta \pm \sqrt{\delta^2+8\kappa^2}\right) \\ 1 \\ 2\kappa/\left(-\delta \pm \sqrt{\delta^2+8\kappa^2}\right) \end{pmatrix} \tag{8}$$

where the waveguide detuning $\delta = \beta_o - \beta_c$ and the corresponding propagation constants

$$\sigma_{1,3} = \frac{\beta_o + \beta_c \pm \sqrt{\delta^2+8\kappa^2}}{2} \tag{9}$$

where σ_1 denotes the fundamental supermode propagation constant.

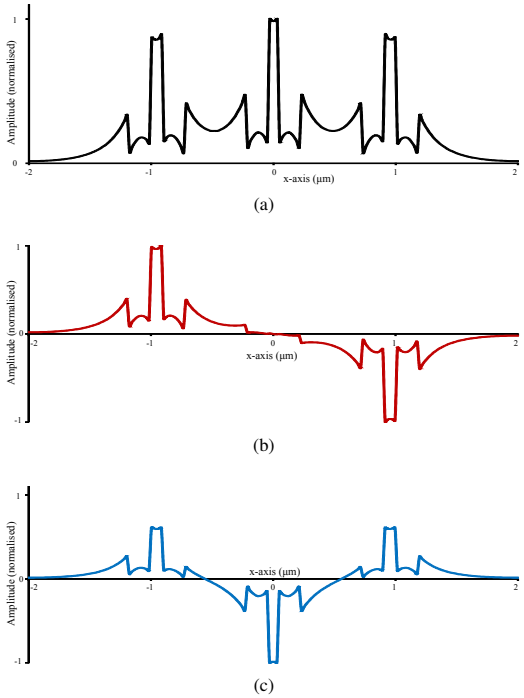

Figure 4: (a) Fundamental supermode profile. (b) 2nd supermode mode profile - Not excited by centre-fed configuration. (c) 3rd supermode mode profile.

The ratio of the peak supermode amplitudes is

$$\gamma = \frac{-\delta + \sqrt{\delta^2 + 8\kappa^2}}{-\delta - \sqrt{\delta^2 + 8\kappa^2}} , \tag{10}$$

which determines the maximum fraction of the power that can be coupled form the centre waveguide to the outside waveguides. In the case of a 3-channel MCDC with identical waveguides, $\beta_o = \beta_c$ and $\delta = 0$ then $\gamma = 1$ and maximum power transfer occurs. On the other hand, a 3-channel DMCDC demonstrates only a very change in the detuning values with almost complete power transfer ($\gamma \approx 0.97$) over a wide range of analyte refractive index values (1.33-1.37).

3.4. Modal propagation analysis

The electric-field profile $\boldsymbol{E}$ at a distance z can be written in terms of the supermode propagation spacings as [18]

$$\boldsymbol{E} = \sum_{v=1,3} E_v \exp\left(-j\left\{\sigma_1 - \sigma_v\right\} z\right) . \tag{11}$$

The supermodes beat along the direction of propagation to form periodic images of the input field.

The corresponding self-image length is given by [18]

$$L = \frac{2\pi}{\sigma_1 - \sigma_3} . \tag{12}$$

Substituting (9) into (12) gives the self-image length in terms of the individual unperturbed waveguide propagation constants β as

$$L = \frac{2\pi}{\sqrt{(\beta_o - \beta_c)^2 + 8\kappa^2}} . \tag{13}$$

This equation shows that the image length is dependent on both waveguide coupling κ and the difference in the unperturbed propagation constants β or the effective indices of the outside and centre waveguides. On the other hand, if we assume that all the waveguides are identical i.e. $\beta_o = \beta_c$ then the structure reduces to a MCDC where the self-image length is given by

$$L = \frac{\pi}{\sqrt{2}\kappa} . \tag{14}$$

Clearly, this shows that the image length of a DMCDC is more sensitive to changes to its waveguides then a MCDC.

3.5. Optical power transmission

The analyte is assumed to infiltrate the gap region between each waveguide. It can be shown that there is an exponential dependence of the coupling on the refractive index of the analyte in this region due to the evanescent fields of the neighbouring waveguides extending into it [11]. Consequently, a change in refractive index of the analyte will result in changes to the coupling coefficient κ between each waveguide. Furthermore, if the analyte infiltrates the slot region of the outside slot waveguides of the DMCDC then the sensor can exploit the strong confinement of light supported by the slot waveguides in this region and the increased sensitivity of the image length of the DMCDC to the resulting change to the outside unperturbed propagation constants β_o. According to (9) these changes will result in a change to the supermode propagation constants σ and from (13) will result in a shift in the self-image length L of the device. This shift in the image relative to its initial position can be related to the power transferred to the output waveguide.

The optical power transmission or transmittance T at a distance z in a waveguide of the DMCDC is calculated from the overlap integral as

$$T(z) = \left(\frac{\int \varepsilon(x,y)\,\psi(x,y)\,dx\,dy}{\sqrt{\int (x,y)^2\,dx\,dy}} \right)^2 , \tag{15}$$

where $\psi(x,y)$ denotes the single mode profile of the output slot waveguide. Consequently, power transfer through the device is sensitive to the interaction between the optical field and the surrounding analyte. So, an DMCDC is a natural interferometer, converting the phase shift in the supermodes to a change in image length and therefore the output power of the MCDC.

3.6. Sensitivity

The sensitivity S of the DMCDC sensor may be defined as the change in transmittance T for a change in the analyte refractive index n_a, and is represented by the curve slope:

$$S_{dmcdc} = \frac{\partial T}{\partial n_a} . \tag{16}$$

For maximum sensitivity, the sensor must be biased to operate at the maximum slope. This corresponds to setting the sensor response in the middle of the linear range or an operating point for which transmittance is 50% of the maximum.

3.7. Design

We selected a centre-fed 3-channel DMCDC for our design. This configuration offers the best performance in terms of sensitivity and dynamic range for device length when compared to other possible configurations [11].

All the device parameters are listed in Table 1. We assumed an operating wavelength of 1550 nm. The sensor device is considered to be built on a silicon-on-insulator platform where the waveguides are located on top of a SiO_2 ($n = 1.444$) buffer layer of height $h_b = 1$ μm; and a Si ($n = 3.476$) substrate. The three slot waveguides and are constructed with Si rail waveguide sections. The slot waveguide dimensions are identical: rail width $w = 180$ nm, slot width $s = 100$ nm, and slot waveguide height $h = 300$ nm. The gap between each slot waveguide is $g = 500$ nm. Furthermore, two outside walls are constructed from SiO_2 to form an analyte container. The walls have a height $h_a = 1.3$ μm, and are a distance $d = 1$ μm away from the slot waveguides.

4. Results

In this section, the performances of a 3-channel DMCDC sensor and a 3-channel MCDC sensor using the design parameters outlined in the previous section are calculated and compared.

Table 1: Sensor design parameters

Parameter	Value
Operating wavelength (λ)	1550 nm
Rail width (w)	180 nm
Slot width (s)	100 nm
Waveguide height (h)	300 nm
Waveguide gap (g)	500 nm
Wall height (h_a)	1.3 μm
Wall distance (d)	1 μm
Buffer height (h_b)	1 μm
Buffer refractive index	1.444 (SiO_2)
Rail refractive index	3.476 (Si)

The supermodes were calculated using a 2-D Full-Vectorial Finite Element method and then used in an Eigen-Mode Propagation technique [20] implemented with COMSOL and MATLAB to simulate the power transfer along the device (Fig. 5).

In order to investigate the sensitivity of each design, simulations were performed and the transmittance T calculated as a function of the analyte refractive index n_a. Operating point were calculated to place the sensor response in the middle of the linear range or 50% transmittance and the corresponding sensitivity S calculated for each.

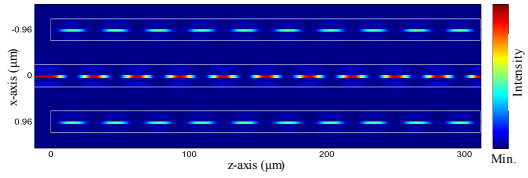

Figure 5: Simulated power evolution (10 self-image lengths) along a centre-fed 3-channel differential multi-channel directional coupler sensor with slot waveguides. This shows a consistent periodic self-imaging phenomenon.

4.1. 3-channel DMCDC sensor

In this design, we assumed that the analyte infiltrates the slot regions of the outside waveguides. The centre waveguide slot region is filled with the material Teflon (n = 1.31) to form the DMCDC structure [8]. A cross section of the 3-channel DMCDC slot waveguide sensor is shown in Fig. 6. The device length was set to 1247 μm, which corresponds to 40 self-image lengths. All other device parameters are listed in Table 1.

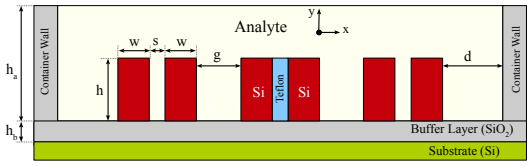

Figure 6: Cross section of a 3-channel differential multi-channel directional coupler with slot waveguides. The analyte is assumed to infiltrate the slot regions of the outside waveguides. The centre slot region is assumed to be filled with Teflon.

The transmittance T was calculated as a function of the analyte refractive index n_a (Fig. 7). We considered two operating points located at an analyte refractive index of 1.3341 and 1.3636. The sensitivity S at these operating points were calculated from Eq. 16 to be S = 285 and S = 645, respectively.

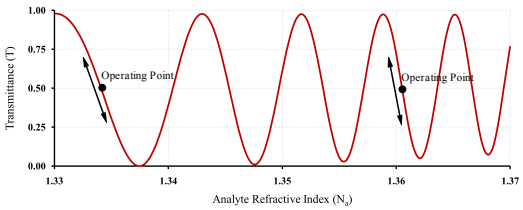

Figure 7: Simulated transmittance T as a function of analyte refractive index n_a for a centre-fed 3-channel differential-channel directional coupler with a device length of 1247 μm. Two operating points for maximum sensitivity are indicated at analyte refractive indices of 1.3341 and 1.3636.

4.2. 3-channel MCDC sensor

In this design, we assumed that the analyte infiltrates the slot region of all three waveguides to form a MCDC structure. A cross section of this 3-channel MCDC slot waveguide sensor is shown in Fig. 8. The device length was set to 1286 μm, which corresponds to 40 self-image lengths. All other device parameters are listed in Table 1.

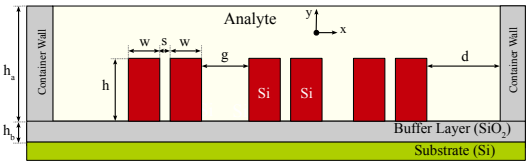

Figure 8: Cross section of a 3-channel multi-channel directional coupler with slot waveguides. The analyte is assumed to infiltrate the slot region of all three waveguides.

The transmittance T was calculated as a function of the analyte refractive index n_a (Fig. 9). We considered two operat-

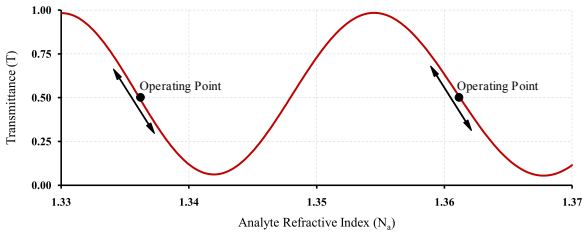

Figure 9: Simulated transmittance T as a function of analyte refractive index n_a for a centre-fed 3-channel differential-channel directional coupler with a device length of 1247 μm. Two operating points for maximum sensitivity are indicated at analyte refractive indices of 1.3341 and 1.3636.

ing points located at an analyte refractive index of 1.3361 and 1.3612. The sensitivity S at these operating points were calculated from Eq. 16 to be $S = 164$ and $S = 170$, respectively.

4.3. Discussion

The operating points and their corresponding sensitivities of both designs are listed in Table 2 for comparison. The responses of both the DMCDC and the MCDC show a change in analyte refractive index that corresponds to a quasi-periodic variation of the transmittance. However, clearly the DMCDC sensor shows a much higher sensitivity than the DMCDC. This verifies the prediction made by the theory in section 3.

Table 2: Comparison of the sensor designs operating point sensitivity

Design	DMCDC	MCDC
Device Length (μm)	1247	1286
Analyte Index	1.3341	1.3361
Sensitivity	285	164
Analyte Index	1.3636	1.3612
Sensitivity	645	170

5. Conclusion

In this work, we described a novel chemical sensor based on a differential multi-channel directional coupler (DMCDC) structure with slot waveguides. The analyte covers the device and infiltrates both the slot regions of the outside waveguides and the spacing between each of the waveguides. The sensitivity of the DMCDC can exploit the exponential dependence of waveguide coupling on the analyte refractive index, the strong confinement of light in the slot regions of the slot waveguides, and the differential nature of the structure. The DMCDC is a natural interferometer, converting the phase shift in the supermodes as a result of an analyte index change, into a change in image length and transmittance of the DMCDC. The transmittance demonstrates a quasi-periodic dependence on analyte index change. This allows the sensor to be tuned by selecting an appropriate device length to fix the operating point at a corresponding sensitivity or by changing the wavelength.

6. References

[1] V. M. N. Passaro, F. Dell'Olio, B. Casamassima, F. De Leonardis, Guided-wave optical biosensors, Sensors 7 (2007) 508–536.

[2] R. Narayanaswamy, O. Wolfbeis, Optical Sensors: Industrial, Environmental and Diagnostic Applications Series, Springer, Heidelberg, 2004.

[3] P. Hua, B. J. Luff, G. R. Quigleya, J. S. W. K. Kawaguchi, Integrated optical dual Mach-Zehnder interferometer sensor, Sens. Actuators, B 87 (2002) 250–257.

[4] C. A. Barrios, K. B. Glyfason, B. Sánchez , A. Griol, H. Sohlström, Holgado, R. Casquel, Slot-waveguide biochemical sensor, Opt. Lett. 32 (2007) 3080–3082.

[5] F. Dell'Olio, V. M. N. Passaro, Optical sensing by optimized silicon slot waveguides, Opt. Express 15 (2007) 4977–4993.

[6] C. A. Barrios, Optical slot-waveguide based biochemcal sensors, Sensors 9 (2009) 4751–4765.

[7] B. J. Luff, R. D. Harris, J. S. Wilkinson, R. Wilson, D. J. Schiffrin, Integrated-optical directional coupler biosensor, Opt. Lett. 21 (8) (1996) 618–620.

[8] V. M. N. Passaro, F. Dell'Olio, C. Ciminelli, M. N. Armenise, Efficient chemical sensing by coupled slot SOI waveguides, Sensors 9 (2009) 1012–1032.

[9] K. R. Kribich, R. Copperwhite, H. Barry, B. Kolodziejczyk, J.-M. Sabattie, K. O'Dwyer, B. D. MacCraith, Novel chemical sensor/biosensor platform based on optical multimode interference (MMI) couplers, Sens. Actuators, B 107 (2004) 188–192.

[10] G. E. Town, R. F. Copperwhite, R. Kribich, K. O'Dwyer, B. MacCraith, Comparison of multimode and multichannel couplers for evanescent sensing of refractive index, in: 30th Australian Conference on Optical Fibre Technology (ACOFT), Sydney, 2005, pp. 1–3.

[11] R. J. McCosker, G. E. Town, Multi-channel directional coupler as an evanescent field optical sensor, Sens. Actuators, B 150 (2010) 417–424.

[12] O. Parriaux, G. Veldhuis, Normalized analysis for the sensitivity optimization of integrated optical evanescent-wave sensors, J. Lightwave Technol. 16 (1998) 573 –582.

[13] R. J. McCosker, G. Town, Chemical sensor using a multi-channel directional coupler with slotwaveguides, in: International Conference on Photonics (ICP), Langkawi, 2010, pp. 1–5.

[14] V. R. Almeida, Q. Xu, C. A. Barrios, M. Lipson, Guiding and confining light in void nanostructure, Opt. Lett. 29 (2004) 1209–1211.

[15] S. R. Somekh, Theory, fabrication and performance of some integrated optical devices, Ph.D. thesis, California Institute of Technology, California (1974).

[16] A. Yariv, Optical Electronics in Modern Communications, Oxford Univ. Press, New York, 1997.

[17] E. Kapon, J. Katz, A. Yariv, Supermode analysis of phase-locked arrays of semiconductor lasers, Opt. Lett. 9 (1984) 125–127.

[18] R. J. McCosker, G. E. Town, Partial image revivals in a multi-channel directional-coupler, Proc. SPIE 7604 (2010) 76040G.

[19] L. B. Soldano, E. C. M. Pennings, Optical multi-mode interference devices based on self-imaging: Principles and applications, J. Lightwave Technol. 13 (1995) 615–627.

[20] D. F. G. Gallagher, T. P. Felici, Eigenmode expansion methods for simulations of optical propagation in photonics - pros and cons, Proc. SPIE 4987 (2003) 69–82.

Pages - of this thesis have been removed as they contain published material. Please refer to the following citation for details of the article contained in these pages.

, . ., , ., , ., & , . (201).
pp p . *r ng h h n ngr , an h n n a n rg ,* 2 , 1.

DOI: 10.13 4/ .2 .

Pages 8-8 of this thesis have been removed as they contain published material. Please refer to the following citation for details of the article contained in these pages.

, . ., , ., , ., & , . (201). p
. *r* , 3 , p. - .

DOI: 10.13 4/ .3 .

The key is to keep company only with people who uplift you, whose presence calls forth your best.

Epictetus

4

Electro-Optic Devices

4.1 Introduction

This chapter presents potential applications of the multi-channel directional coupler (MCDC) structure using the recently discovered electro-optic crystal OH1 [Hunziker et al., 2008b] and the recently developed electro-optic polymer CLD-1/APC [Zhang et al., 2001] for electro-optic devices, i.e. optical electric field sensors, switches and modulators.

Initially, we extended our work using the MCDC structure for optical evanescent field sensing (see Chapter 3) with the idea of replacing the analyte that infiltrates the spacing between the waveguides with an electro-optic material to create an optical electric

field sensor. The sensor utilises the linear electro-optic effect, where the application of an electric field will modify the coupling between the waveguides. The resulting work is presented as the first publication in this chapter: *"Optical Electric Field Sensor using a Multi-Channel Directional Coupler"* [McCosker and Town, 2010h].

Following this, we extended the design by adding electrodes to the structure in order to form a delta-κ electro-optic switch. The description delta-κ refers to the fact that the electro-optic material is used as the cladding layer that infiltrates the spacing between the waveguides and therefore the application of an electric field across the electro-optic cladding will result in a change in the coupling coefficient ($\Delta\kappa$). The resulting work is presented as the second publication in this chapter: *"An Electro-Optic Switch Based on a Multi-Channel Directional Coupler"* [McCosker and Town, 2010d].

Next, we considered the design as a high speed electro-optic delta-κ modulator. To do this we had to extend the analysis to consider velocity matching the microwave and optical guided waves. The resulting work is presented as the third publication in this chapter: *"A Delta-K Electro-Optic Polymer Modulator using a Multi-Channel Directional Coupler"* [McCosker and Town, 2010c].

Finally, instead of using an electro-optic cladding layer to form a delta-κ modulator, I considered using the electro-optic material as the waveguide cores of the MCDC to form a delta-β modulator. The description delta-β refers to the fact that the electro-optic material is used for the waveguide cores and therefore the application of an electric field will result in the introduction of a phase mismatch ($\Delta\beta$) between the optical fields in the waveguides. The resulting work is presented as the final publication of this chapter: *"An Electro-Optic Modulator using a Multi-Channel Directional Coupler with a Poled Electro-Optic Polymer"* [McCosker and Town, 2010a].

4.2 Publications

The remaining chapter consists of the following four publications:

1. Ravi J. McCosker and Graham E. Town, **Optical Electric Field Sensor using a Multi-Channel Directional Coupler**, submitted to *IEEE Sensors Journal*.

2. Ravi J. McCosker and Graham E. Town, **An Electro-Optic Switch Based on a Multi-Channel Directional Coupler**, in *Proceedings of the 35th Australian Conference on Optical Fibre Technology (ACOFT)*, Melbourne, 2010.

3. Ravi J. McCosker and Graham E. Town, **A Delta-K Electro-Optic Polymer Modulator using a Multi-Channel Directional Coupler**, in *Proceedings of the International Conference on Electromagnetics in Advanced Applications (ICEAA)*, Sydney, 2010, pp. 859-862.

4. Ravi J. McCosker and Graham E. Town, **An Electro-Optic Modulator using a Multi-Channel Directional Coupler with a Poled Electro-Optic Polymer**, in *Proceedings of the Third International Conference on Communications and Electronics (ICCE)*, Nha Trang, 2010, pp. 329-334.

Optical Electric Field Sensor using a Multi-Channel Directional Coupler

Ravi J. McCosker, *Student Member, IEEE,* and Graham E. Town, *Senior Member, IEEE.*

***Abstract*—We describe a novel structure for electric field sensing based on a multi-channel directional coupler with an electro-optic cladding that infiltrates the spacing between the individual waveguides. The electric-field sensor utilises the electro-optic effect to modify the coupling between the waveguides and hence the optical transmittance of the device. This electric field sensor does not require electrodes. Since the device is all-dielectric, there is only minimal disturbance to the field being measured and complete electrical isolation.**

***Index Terms*—multi-channel directional coupler, electric field, sensor, electro-optic.**

Integrated electro-optic sensors for electric field measurement were first proposed over 25 years ago [1], [2]. The now well establish Mach-Zehnder interferometer configuration was used and implemented in lithium niobate [1]. Typically this configuration requires metal electrodes to be placed near one or both waveguides in the interferometer to direct the field and apply it to the region of the electro-optic material [1], [3]–[5]. Alternate designs proposed include: Fabry-Pèrot cavities [6], Bragg grating in lithium niobate [7], cutoff modulators with dummy electrode structures [8], and electro-optically tuned directional couplers [9].

For high voltage measurements two approaches have been proposed. In the first, the sensor employs a capacitive voltage divider, which is used to divide out a small voltage which can be directly applied to the sensor via electrodes. However, the presence of the conductive parts creates several problems, including perturbation of the field to be measured, bandwidth limitations and the potential for catastrophic breakdown [10]. In order to overcome these limitations, the second approach directly immerses the device in the electric field to be measured [11], [12].

I. Multi-Channel Directional Coupler

A multi-channel directional coupler (MCDC) [13] consists of an array of identical and equally spaced channel waveguides buried in a cladding layer, as outlined in the schematic of Fig. 1. The waveguides are in sufficiently close proximity that they may be considered to be a coupled system rather than an array of individual waveguides. Incident light focused into the input or feed waveguide will couple into the adjacent waveguides.

Supermodes [14], are eigenmodes of coupled (waveguide) systems. They may be derived by diagonalisation of the matrix describing the coupling between the unperturbed modes of the individual waveguides. A system of N weakly coupled waveguides can be regarded as supporting N supermodes, each with a constant amplitude and unique propagation constant. Together the supermodes beat to form a multi-mode interference (MMI) pattern along the direction of propagation of the device. As a result, the input field is revived or imaged at periodic intervals along the device.

Ravi J. McCosker is with the Department of Electronic Engineering, Macquarie Unviersity, NSW 2109, Australia. email: ravi.mccosker@mq.edu.au

Manuscript received November 23, 2010.

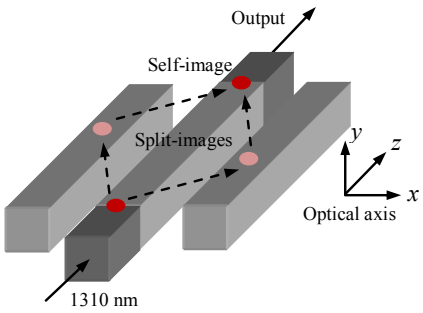

Fig. 1. Schematic of a centre-fed 3-channel multi-channel directional coupler with single input and single output ports indicated. A split-image and self-image of the input field are also shown.

Using supermodes, the MCDC can be described as a single composite waveguide structure that support multiple modes or supermodes [15]. The operation of the MCDC can then be analysed in terms of MMI for periodic imaging [16].

II. Theory and Design

In this work, we will consider a 3-channel MCDC structure. This is based on our previous work on evanescent field sensors [17], where we showed that the 3-channel MCDC offers the greatest sensitivity per unit length when compared to the directional coupler structure and other various MCDC channel variations. Furthermore, we selected a centre-fed configuration, ie. the input is fed to the centre waveguide of the array. A centre-fed configuration is used to prevent partial image revivals [18], which have been shown to degrade sensor performance.

A. Theory

The 3-channel MCDC supports three supermodes. However, the centre-fed configuration only excites the two odd, symmetric modes. If we assume that the waveguides are far enough apart that only adjacent waveguides in the array couple then the supermode propagation constants σ are given by

$$\sigma_1 = \beta + \sqrt{2}\kappa \; ; \qquad \sigma_3 = \beta - \sqrt{2}\kappa \; ; \tag{1}$$

where β denotes the propagation constant common to each unperturbed waveguide; κ denotes the common coupling coefficient; and σ_1 denotes the fundamental supermode propagation constant. Consequently, the supermode propagation constants depend on the waveguide coupling.

The image length can be written in terms of the beat length or supermode propagation spacing as [18]

$$L = i\,\frac{\pi}{\sigma_1 - \sigma_3} \qquad i > 0\,, \tag{2}$$

where i is an integer whose parity determines whether the image is either a split-image (odd) or a self-image (even); as indicated in Fig. 1. Alternatively, by substituting (1) into (2), the image length L can be written in terms of the coupling coefficient κ as

$$L = i\,\frac{\pi}{2\sqrt{2}\kappa} \qquad i > 0\,. \tag{3}$$

Equation (3) shows that the device image length L is dependant on waveguide coupling. The coupling κ between two symmetric waveguides can be approximated by [19]

$$\kappa = 2\sqrt{n_w^2 - n_c^2}\,\frac{k}{\beta w_{\text{eff}}}\exp\left[-\sqrt{\beta^2 - (n_c k)^2}\left(s + \frac{w}{2}\right)\right]\,, \tag{4}$$

where w is the waveguide width; s is the waveguide separation; n_w is the waveguide refractive index; n_c is the cladding refractive index; β is the unperturbed propagation constant common to each waveguide; w_{eff} is the effective waveguide width; and k is the wavenumber.

Equation (4) shows that there is an exponential dependence of the coupling on the refractive index of the surrounding cladding. So, if the cladding material infiltrates the region between the coupled waveguides then the device can exploit this exponential dependence of the coupling on the cladding index. Referring to (3), changes to the refractive index of the cladding material will cause a shift in the image length, and therefore the power transmitted to the output (i.e. centre waveguide) of the MCDC device. By making the cladding material that infiltrates the spacings between the waveguides an electro-optic material, the MCDC can become a sensitive electric field sensor.

B. OH1 organic electro-optic crystal

As an example demonstrating the potential performance of this structure we have modelled the device with a cladding material consisting of the organic nonionic molecular crystal OH1 (2-(3-(4-hy-droxystyryl)-5,5-dimethylcyclohex-2-enylidene)malononitrile). The potential of the OH1 molecule for applications in electro-optics has only recently been discovered [20]–[22]. OH1 is a novel nonlinear electro-optical biaxial crystal, with orthorhombic symmetry (point group $mm2$) [21]. OH1 crystals show a low absorption $< 0.3\ mm^{-1}$ over a large wavelength range between 680 and 1460 nm [23]. Single crystalline thin films with a very large area of more than 2 cm^2 and thickness between 0.1-4 μm have been fabricated on amorphous substrates, including glass and silicon on insulator [21]. These films exhibited very large electro-optic coefficients, e.g., $r_{33} = 104$ pm/V at 633 nm and $r_{33} = 52$ pm/V at 1319 nm, leading to very large electro-optic figures of merit of more than 500 pm/V in the whole transparency range [23].

The OH1 film may be deposited so that its polar axis (x_1, x_2, x_3) is aligned, as indicated in Fig. 2. This allows us to take advantage of the electro-optic effect with the largest coefficient r_{33} for propagating TM-modes, for which the electric field oscillates in the y-axis of the device. The application of an external electric field E_3 (i.e. parallel to the y-axis of the device or x_3-axis of the crystal) induces a proportional change in the crystal's refractive index as a result of the Pockels effect or linear electro-optic effect. The change in refractive index is given by

$$\Delta n_y = \frac{1}{2} n_y^3 r_{33} E_3\,. \tag{5}$$

C. Design

The device was designed to operate at 1310 nm, for which OH1 exhibits the highest electro-optic coefficient $r_{33} = 52$ pm/V for the optical telecommunications bands [23]. A cross section of the 3-channel MCDC is shown in Fig. 2. The device is composed of 3 identical waveguides of cross section 4×4 μm (w×h) for single mode operation. The array waveguides are assumed to be composed of a material with a refractive index of 1.59. The waveguides are located on top of a glass substrate with a refractive index of 1.44. The array waveguides are covered by an electro-optic cladding layer, which is assumed to infiltrate the spacing between the waveguides. The cladding layer has a height $h_{clad} = 9$ μm and extends a distance $d = 5$ μm away from the outer array waveguides. The electro-optical material is assumed to be OH1, which has a refractive index of 1.58 [23].

Device sensitivity was maximized by optimizing waveguide coupling changes to an applied electric field. This was done by varying the waveguide spacing s between $1 - 3.5$ μm and calculated the coupling coefficient κ in the absence of an applied electric field $E_a = E_3 = 0\,Vcm^{-1}$ and for an applied electric field $E_b = E_3 = 10\ kVcm^{-1}$. The device length was maintained at around 8 cm in order to correspond to an integer image rank N, i.e. number of images along the propagation length of the device. The supermodes of the device were calculated using a Finite Element Method and applied to (2) to calculate the corresponding image length L; and (3) to calculate the corresponding coupling coefficient κ. The resulting coupling κ values were plotted against their corresponding waveguide spacing s, as shown in Fig. 3.

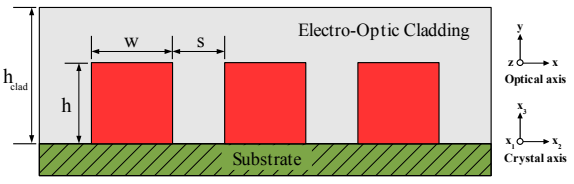

Fig. 2. A cross section of the 3-channel multi-channel directional coupler sensor. The optical axis and crystal axis are also indicated.

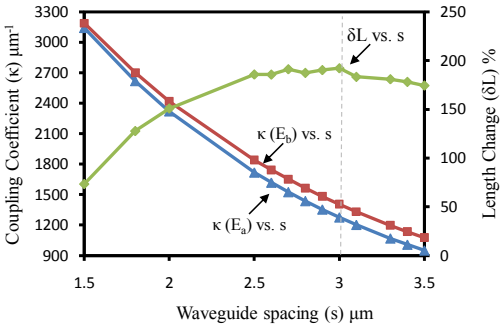

Fig. 3. Plot of coupling (κ) and length change (δL) vs. waveguide spacing (s).

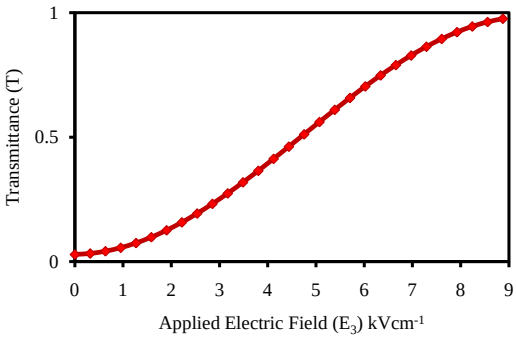

Fig. 5. Transmittance (T) vs. applied electric field E_3.

The results show that for a given image rank an increase in waveguide spacing corresponds to an increase in the change in coupling and hence an increase in the change in image length due to an applied electric field. This corresponds to a a higher device sensitivity to electric field changes. On the other hand, an increase in waveguide spacing also corresponds to an increase in overall device length and therefore decrease in image rank. For constant coupling, sensitivity scales with image rank [17], i.e. an decrease in image rank results in an decrease in sensitivity. Thus the overall resulting sensitivity has to be considered. In order to do this, we calculated the percentage length change δL, which is a function of both image rank N and change in image length due to an applied electric field; and is given by

$$\delta L = N \frac{L(E_a) - L(E_b)}{L(E_a)} \times 100 \tag{6}$$

where $L(E_a)$ is the image length without applied field and $L(E_b)$ is the image length with the applied electric field E_b. The percentage length change δL was plotted against waveguide spacing s as shown in Fig. 3. The results show that maximum device sensitivity occurs at a waveguide spacing of $s = 3$ μm. Using this and the device parameters outlined previously, a centre-fed 3-channel MCDC sensor was designed with a device length of 8.12 cm.

III. Results and Discussion

We used an Eigen-Mode propagation technique [24] implemented with COMSOL and MATLAB to simulate the evolution of the input field along the device for a quasi-TM mode at 1310 nm. The simulated field evolution of the device for an applied electric field $E_3 = 9\ kVcm^{-1}$ is shown in Fig. 4.

Furthermore, the sensing characteristic represented as the variation in optical transmittance T as a function of the applied electric field E_3 is shown in Fig. 5. The results show a measurement range of 9 $kVcm^{-1}$.

Since temperature dependence figures were not available for the electro-optic material OH1 we had to ignore any effects of temperature on both device sensitivity and bias. We note that in the case of light propagation along the optical axis (z-axis) of a device and electric field applied perpendicularly to this (y-axis), temperature dependence has been shown to be negligible in other structures [25]. The influence of temperature and polarization will be explored in a future publication that examines a fabricated version of the device.

One possible application of our electric-field sensor would be the detection and measurement of transients on high-voltage lines. Electric fields up to 7 $kVcm^{-1}$ are encountered in SF_6-insulated bus ducts under normal operating conditions [26]. Larger instantaneous fields can occur during and following breakdown events. As sensitivity scales with device length, a shorter device could measure a larger range of electric fields. Our sensor could be redesigned to monitor

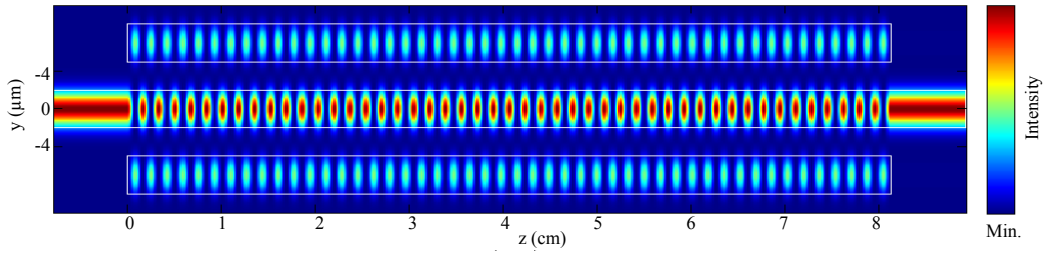

Fig. 4. Field evolution of the centre-fed 3-channel multi-channel directional coupler sensor for an applied electric field $E_3 = 9\ kVcm^{-1}$. Device length L is 8.12 cm. Image rank N is 48.

under breakdown conditions a high voltage line, for which transients with electric field peaks of up to 21 $kVcm^{-1}$ can occur.

IV. Conclusion

In conclusion, we have described an electric field sensor based on a centre-fed 3-channel multi-channel directional coupler structure. The device employs an organic electro-optic crystal OH1 as the cladding layer. The electro-optic cladding layer infiltrates the spacing between the waveguides and therefore the device can exploit the exponential dependence of the coupling on the cladding refractive index. A sensor was designed and optimised for maximum sensitivity. For an 8.12 cm device the measurement range was 9 $kVcm^{-1}$.

References

[1] C. H. Bulmer, W. K. Burns, and R. P. Moeller, "Linear interferometric waveguide modulator for electromagnetic-field detection," *Opt. Lett.*, vol. 5, pp. 176–178, 1980.

[2] V. M. N. Passaro, F. Dell'Olio, and F. D. Leonardis, "Electromagnetic field photonic sensors," *Prog. Quant. Electron.*, vol. 30, pp. 45–73, 2006.

[3] M. J. Ahmed and L. Young, "Mach-Zehnder interferometer tuning with Ta_2O_5 film loading," *Appl. Opt.*, vol. 22, pp. 4082–4087, 1983.

[4] N. A. F. Jaeger and L. Young, "High-voltage sensor employing an integrated optics Mach-Zehnder interferometer in conjunction with a capacitive divider," *J. Lightwave Technol.*, vol. 7, pp. 229 – 235, 1989.

[5] R. Zeng, Y. Zhang, W. Chen, and B. Zhang, "Measurement of electric field distribution along composite insulators by integrated optical electric field sensor," *IEEE Trans. Dielectr. Electr. Insul.*, vol. 15, pp. 302 –310, 2008.

[6] M.-S. Huanga, M.-H. Lu, and J.-T. Shy, "High sensitivity bulk electro-optic modulator field sensor for high voltage environments," *Rev. Sci. Instrum.*, vol. 75, p. 5364, 2004.

[7] D. Runde, S. Brunken, C. E. Rüter, and D. Kip, "Integrated optical electric field sensor based on a Bragg grating in lithium niobate," *Appl. Phys. B*, vol. 86, pp. 91–95, 2007.

[8] S. S. Lee, M. C. Oh, S. Y. Shin, and K. H. Keh, "Integrated optical high-voltage sensing using z-cut $LiNbO_3$ cutoff modulator," *IEEE Photonics Technol. Lett.*, vol. 5, p. 996, 1993.

[9] M. M. Howerton, C. H. Bulmer, and W. K. Burns, "Linear 1×2 directional coupler for electromagnetic field detection," *Appl. Phys. Lett.*, vol. 52, pp. 1850–1852, 1988.

[10] F. Rahmatian and J. N. Blake, "Applications of high-voltage fiber optic current sensors," *IEEE PES General Meeting*, 2006.

[11] A. Nicolas, F. Jaeger, and L. Young, "Asymmetric slab and stri-loaded integrated optic devices for the measurement of large electric fields," *J. Lightwave Technol.*, vol. 5, pp. 745–750, 1987.

[12] D. H. Naghski, J. T. Boyd, H. Jackson, S. Sriram, S. A. Kingsley, and J. Latess, "An integrated photonic Mach-Zehnder interferometer with no electrodes for sensing electric field," *J. Lightwave Technol.*, vol. 12, pp. 1092 – 1098, 1994.

[13] S. R. Somekh, *Theory, fabrication and performance of some integrated optical devices*. PhD thesis, California Institute of Technology, California, 1974.

[14] A. Yariv, *Optical Electronics in Modern Communications*. Oxford Univ. Press, New York, 1997.

[15] E. Kapon, J. Katz, and A. Yariv, "Supermode analysis of phase-locked arrays of semiconductor lasers," *Opt. Lett.*, vol. 9, pp. 125–127, 1984.

[16] L. B. Soldano and E. C. M. Pennings, "Optical multi-mode interference devices based on self-imaging: Principles and applications," *J. Lightwave Technol.*, vol. 13, pp. 615–627, 1995.

[17] R. J. McCosker and G. E. Town, "Multi-channel directional coupler as an evanescent field optical sensor," *Sens. Actuators, B*, vol. 150, pp. 417–424, 2010.

[18] R. J. McCosker and G. E. Town, "Partial image revivals in a multi-channel directional-coupler," *Proc. SPIE*, vol. 7604, p. 76040G, 2010.

[19] K. J. Ebeling, *Integrated Optoelectronics: Waveguide Optics, Photonics, Semiconductors*. Springer-Verlag, 2003.

[20] F. D. Brunner, O.-P. Kwon, S.-J. Kwon, M. Jazbinšek, A. Schneider, and P. Günter, "A hydrogen-bonded organic nonlinear optical crystal for high-efficiency terahertz generation and detection," *Opt. Express*, vol. 16, pp. 16496–16508, 2008.

[21] C. Hunziker, S.-J. Kwon, H. Figi, F. Juvalta, O.-P. Kwon, M. Jazbinšek, and P. Günter, "Configurationally locked, phenolic polyene organic crystal 2-{3-(4-hydroxystyryl)-5, 5-dimethylcyclohex-2-enylidene} malononitrile: linear and nonlinear optical properties," *J. Opt. Soc. Am. B*, vol. 25, pp. 1678–1683, 2008.

[22] O.-P. Kwon, S.-J. Kwon, M. Jazbinšek, F. D. J. Brunner, J.-I. Seo, C. Hunziker, A. Schneider, H. Yun, Y.-S. Lee, and P. Günter, "Organic phenolic configurationally locked polyene single crystals for electro-optic and terahertz wave applications," *Adv. Funct. Mater.*, vol. 18, pp. 3242–3250, 2008.

[23] C. Hunziker, M. Jazbinšek, S.-J. Kwon, O.-P. Kwon, H. Figi, and P. Günter, "Electro-optic modulation in high-efficiency crystalline oh1 optical waveguides," in *Conference on Lasers and Electro-Optics/International Quantum Electronics Conference*, 2009.

[24] D. F. G. Gallagher and T. P. Felici, "Eigenmode expansion methods for simulations of optical propagation in photonics - pros and cons," *Proc. SPIE*, vol. 4987, pp. 69–82, 2003.

[25] V. M. Gaba, D. Y. Sugak, and I. M. Kravchuk, "Possible application of $LiNbO_3$ single crystals as temperature indicators based on the temperature dependencies of the birefringence," *Proc. SPIE*, vol. 2795, pp. 321–324, 1996.

[26] T. Kobayashi, S. Mari, M. Koshiishi, K. Nimomiya, M. Matsuki, H. Yokoyama, and T. Hara, "Development of compact 500-kV 8000-A gas insulated transmission line-study on insulation design," *IEEE Trans. Power. App. Syst.*, vol. PAS-103, pp. 3154–3162, 1984.

Ravi J. McCosker received his LLB BSc (Hons I) in 2006, and is currently working toward a Doctor of Philosophy from the Department of Electronic Engineering, Macquarie University, Australia. His research interests include optical sensors, electro-optic devices, digital signal processing, rf and microwave design.

Graham Town graduated with a Bachelor of Engineering (Hons I) in electrical engineering from the NSW Institute of Technology (now University of Technology, Sydney) in 1984, and graduated as Doctor of Philosophy from the University of Sydney, Australia, in 1992. From 1991 to 2002 he was employed as an academic in the Department of Electrical Engineering at the University of Sydney where he conducted research in the areas of magnetic resonance imaging, and subsequently in optical fibre lasers and photonics. He is currently Professor in Electronic Engineering at Macquarie University, Sydney, Australia, where he initiated and developed the University's undergraduate engineering program. His current research interests are in guided-wave optical devices and their applications in telecommunication and sensing. Professor Town is currently a member of the Australian Optical Society, OSA, and Engineers Australia. He has served as chairperson of the NSW joint chapter of IEEE MTT/APS, was founding chairperson of the NSW chapter of IEEE LEOS, and is currently chairperson of the NSW joint chapter of IEEE Photonics/SSC/CAS.

, . ., & To , . . (201). n Electro-Optic Switch Based on a Multi-Channel Directional Coupler. *35th Australian Conference on Optical Fibre Technology, Melbourne, VIC, 2010,* p. 1-3.

DOI: 10.1 9/ACOFT.2 . 929924

, . ., & To , . . (201). - - p p
- p . *n rna na n r n n r agn n*
an a n , 2 , p. 9- 2.

DOI: 10.1 9/ .2 . 3224

McCosker, R. J., & Town, G. E. (2010). An electro-optic modulator using a multi-channel directional coupler with a poled electro-optic polymer. *International Conference on Communications and Electronics, Nha Trang 2010*, p. 329-334.

DOI: 10.1109/ICCE.2010.5670657

We shall not cease from exploration
And the end of all our exploring
Will be to arrive where we started
And know the place for the first time.

T. S. Eliot,
Four Quartets: Little Gidding

5 Conclusions

The research presented in this thesis concerned the analysis and design of multi-channel directional coupler (MCDC) structures for potential applications in sensing and electro-optic devices.

5.1 Synthesis

In chapter 2, the first publication "*Partial Image Revivals in a Multi-Channel Directional Coupler*" [McCosker and Town, 2010i] analysed the MCDC using the theory of super-modes. A potential limitation inherent in the MCDC structure was identified with the discovery of the phenomenon of partial image revivals. If we bring the waveguides

in the array closer together then we increase the coupling between the waveguides themselves. The increased coupling results in a quicker transfer of energy between the waveguides and hence shorter image lengths. However, as the waveguides get close enough together the effect of coupling between non-adjacent waveguides becomes significant. In this case, the power evolution of the MCDC begins to exhibit a more complex interference pattern between the higher order supermodes. The result is the formation of what we call partial image revivals at periodic intervals along the direction of propagation of the MCDC. These periodic partial images quickly fade out and then re-emerge along the device to form a complete image. This results in a significant increase in the image length of the complete images of the input field making compact devices difficult to implement.

In chapter 2, the second publication, "*Multi-Channel Directional Coupler for WDM in Fluorescence Sensing*" [McCosker and Town, 2010f] described the exploitation of the phenomenon of partial image revivals to design a compact 1×2 WDM for fluorescence sensing using a MCDC structure. The WDM is designed to be a 'front-end' for a compact fluorescence sensing system that is integratable, e.g. in a 'lab-on-a-chip'. We showed that it is possible to take advantage of the partial image revivals that occur near complete images (as they are themselves almost complete images) to design a compact device. The design highlights a trade-off between device length and isolation ratio. Although we used a partial self-image to extract the 692 nm pump to the fluorophore/analyte for a more compact device, the trade-off was a reduced isolation ratio when compared to the extraction of the 712 nm excitation signal to the detector, which used a complete mirror-image.

In chapter 3, the first publication "*Multi-Channel Directional Coupler as an Evanescent Field Optical Sensor*" [McCosker and Town, 2010e] described the application of

the MCDC structure for evanescent field optical sensing using polymer planar waveguides. If the analyte is allowed to infiltrate the spacing between the coupled waveguides then the sensor can exploit the exponential dependence of the coupling on the analyte refractive index. These sensors may be regarded as detecting an effective index change in the supermodes of the composite waveguide structure. This approach has the advantage of modulating the device transmittance with analyte index through interference between the supermodes of the structure, providing a simpler and more robust interferometric sensing platform than a Mach-Zehnder. Due to the large differential overlap of the supermodes with the analyte they can achieve high sensitivity, and by exploiting the exponential dependence of the coupling on the analyte refractive index they can be designed to provide high sensitivity and/or large dynamic range in a single device. The quasi-periodic dependence of coupling on analyte refractive index allows the sensor performance to be tuned by selecting an appropriate device length to fix the operating point at a corresponding sensitivity.

In chapter 3, the first publication [McCosker and Town, 2010e] also analysed the MCDC structure to identify the optimum configuration for sensitivity. It was shown that the larger the number of waveguides (channels) in a MCDC sensor the more significant is the impact of the phenomenon of partial image revivals on the output power transmission of the sensor. Furthermore, when more than three waveguides are used the periodic complete image revivals that normally occur along the direction of propagation of the MCDC sensor are replaced by a series of periodic partial image revivals, which can be seen as a dampened out series of undulations in the transmission response. The result is that although adding more channels to a MCDC does increase the sensitivity, this also results in an increase in device length and the appearance of partial images along the device. Subsequently, when we consider sensitivity verses de-

vice length, the 3-channel MCDC is the optimum configuration for a sensor design, i.e. highest sensitivity per unit length. In particular, a centre-fed 3-channel MCDC avoids partial image revivals altogether, which is a result of the fact that only two supermodes are excited and therefore higher order supermode beating is avoided.

In chapter 3, the second publication "*Optical Chemical Sensor using a Multi-Channel Directional Coupler with Slot Waveguides*" [McCosker and Town, 2010g] described a novel optical chemical sensor based on a MCDC with silicon slot waveguides. We showed that the sensitivity of the MCDC can be enhanced by using slot waveguides. If the analyte is allowed to infiltrate both the spacing between the coupled waveguides and the slots of the waveguides themselves then the sensor can exploit the high confinement of light in the slots to enhance the overall sensitivity of the sensor, whilst retaining the exponential dependence of the coupling on the analyte refractive index.

In chapter 3, the third publication "*Optical Chemical Sensor using a Differential Multi-Channel Directional Coupler with Slot Waveguides*" [McCosker and Town, 2010g] described an optical chemical sensor using a new structure that was referred to as a differential multi-channel directional coupler (DMCDC). The DMCDC was defined as a MCDC that consists of an odd number of waveguides (channels), where all waveguides are equally spaced and identical, except the centre waveguide. This structure represents the most efficient configuration for the MCDC, i.e. higher sensitivity and shorter device length. The work showed that a chemical sensor that used the DMCDC structure with silicon slot waveguides resulted in an increase in sensitivity of almost four times when compared to a MCDC version of the sensor with slot waveguides.

In chapter 3, the final publication "*Microstructured Optical Fiber Refractive Index Sensor*" [Town et al., 2010b] described an equivalent MCDC structure in fiber for refrac-

tive index sensing of an analyte. The design implemented an array of coupled waveguides as a dual-core microstructured optical fiber for which the transmittance is highly sensitive to the refractive index of the holes. We showed that selective filling of the microstructure with analyte can increase the device sensitivity by approximately one order of magnitude.

In chapter 4, the first publication "*Optical Electric Field Sensor using a Multi-Channel Directional Coupler*" [McCosker and Town, 2010h] described an optical electric field sensor based on a MCDC structure with an electro-optic cladding. Since the cladding material that infiltrates the spacing between the coupled waveguides is an electro-optic material, the device can exploit the exponential dependence of the coupling on the cladding refractive index to become an electric field sensor. The sensor uses the Pockels effect to modify the coupling between the array waveguides in the presence of an electric field, and hence the optical transmittance of the device. The sensor is all dielectric, i.e. it does not require metal electrodes to be placed near one or all of the waveguides to direct the field and apply it to the region of the electro-optic material. Thus, there is only minimal disturbance to the field being measured and complete electrical isolation. On the other hand, without the presence of electrodes to direct the field, the sensitivity of this sensor is quite weak. In order to obtain a measurement range of 9 kV/cm the sensor required a length of 8.12 cm.

In chapter 4, the second publication "*An Electro-Optic Switch Based on a Multi-Channel Directional Coupler*" [McCosker and Town, 2010d] described a delta-κ electro-optic switch using the MCDC structure with an electro-optic cladding material. The description delta-κ refers to the fact that the electro-optic material is used as the cladding layer that infiltrates the spacing between the waveguides and therefore the application of an electric field across the electro-optic cladding will result in a change in the

coupling coefficient ($\Delta\kappa$). We assumed the electro-optic material was the recently discovered organic electro-optic crystal, OH1 [Hunziker et al., 2008b]. This electro-optic material has an electro-optic coefficient of 52 pm/V and a refractive index of 1.58 at 1310 nm [Hunziker et al., 2008b]. This allowed the MCDC switch to employ a simple microstrip travelling wave electrode structure. The results showed that a switch of length 3.3 cm demonstrated a switching time of only 171 ps. Nevertheless, the device required a large switching voltage of 11.2 V across the electrodes to switch the signal to the opposite output waveguide port. The advantage of the MCDC as a switch was the large resulting 3-dB bandwidth, in this case 20 nm.

In chapter 4, the third publication *"A Delta-K Electro-Optic Polymer Modulator using a Multi-Channel Directional Coupler"* [McCosker and Town, 2010c] described the design of a high speed electro-optic delta-κ modulator using the MCDC structure. We assumed the electro-optic material was the recently developed electro-optic polymer CLD-1/APC [Zhang et al., 2001]. This electro-optic material has an electro-optic coefficient of 170 pm/V and a refractive index of 1.614 at 1310 nm [Shi et al., 2000a]. It also has many advantages that aid a high speed electro-optic modulator design. For instance, the response time of the electro-optic polymer material is so fast (measured in femto-seconds) that it can reasonably be concluded that there is no delay between the signal and the change in the refractive index. Furthermore, polymers have a very low loss tangent, tan $\delta \sim 10^{-4}$ up to 400 GHz and therefore dielectric loss is insignificant [Lee et al., 2002a]. Thus, our analysis showed that if the device is velocity and impedance matched then the 3-dB bandwidth of the device was determined by conductor loss alone. The results showed that a device 5.25 mm long demonstrated a 3-dB bandwidth of 176 GHz. However, again as in the previous switch design the drive voltage required was quite large at 16.5 V.

In chapter 4, the final publication *"An Electro-Optic Modulator using a Multi-Channel Directional Coupler with a Poled Electro-Optic Polymer"* [McCosker and Town, 2010a] described the design of a high-speed electro-optic delta-β modulator using the MCDC structure. The description delta-β refers to the fact that the electro-optic material is used for the waveguide cores and therefore the application of an electric field will result in the introduction of a phase mismatch ($\Delta\beta$) between the optical fields in the waveguides. Once again, we assumed the electro-optic material was the recently developed electro-optic polymer CLD-1/APC [Zhang et al., 2001]. The work discussed creating an intrinsic push-pull structure using the fact that the electro-optic material is poled, i.e. the application of an electric field will result in an increase in the refractive index of the outside waveguides, while the refractive index of centre waveguide decreases (or vise versa). This formed the basis for my discovery of the DMCDC structure (see Chapter 3). The problem raised in this publication was whether to initially pole the electro-optic material to form an intrinsic push-pull structure, which then only required a simple microstrip electrode structure; or implement a complex strip-line electrode structure, which avoided the issue of how to initially pole the individual waveguides. Neither solutions seem plausible in terms of producing a low cost and easy to fabricate device. Thus, although the results showed that a device of length 3.78 mm demonstrated a 3-dB bandwidth of 231 GHz with a drive voltage of only 1.9 V, the practical use of the intrinsic push-pull structure for a low cost, large bandwidth and low drive voltage modulator is not plausible with this structure.

5.2 Contributions

In conclusion, the research presented in this thesis makes the following contributions to the knowledge and understanding of the field:

- the identification and analysis of the phenomenon of partial image revivals in terms of the theory of supermodes [McCosker and Town, 2010i];
- exploitation of the phenomenon of partial image revivals to design a compact WDM for fluorescence sensing [McCosker and Town, 2010f];
- the design of a novel evanescent field optical sensor using the MCDC structure and polymer planar waveguides [McCosker and Town, 2010e];
- the design of a novel optical chemical sensor using the MCDC structure and silicon slot waveguides [McCosker and Town, 2010b];
- the discovery of the differential multi-channel directional coupler (DMCDC) structure and its use as an efficient optical chemical sensor using silicon slot waveguides [McCosker and Town, 2010g];
- the design of an all-dielectric optical electric field sensor based on a MCDC structure [McCosker and Town, 2010h];
- the design of a delta-κ electro-optic switch using the MCDC structure and the recently discovered electro-optic crystal OH1 [McCosker and Town, 2010d];
- the investigation and design of electro-optic modulators based on the MCDC structure using the recently developed electro-optic polymer CLD-1/APC and the electro-optic crystal OH1 [McCosker and Town, 2010d,a,c]

5.3 Future Work

The research in this thesis has resulted in some interesting directions for future research. For example, the evanescent field optical sensor designed in the first publication of Chapter 3 [McCosker and Town, 2010e] should be fabricated in a polymer, planar waveguide technology and tested. Furthermore, the chemical sensors designed in the second and third publications of Chapter 3 [McCosker and Town, 2010b,g] should also be fabricated and tested. In particular, the question needs to be answered whether or not an analyte can infiltrate the 100 nm slots of the waveguides? In addition, research needs to be conducted to determine what influence fabrication errors have on the transmittance of all of these sensors.

Preliminary research not included in this thesis has shown that by using a DMCDC structure and slot waveguides, the optical electric field sensor designed in the first publication of Chapter 4 [McCosker and Town, 2010h] can be significantly improved, i.e. the device length can be reduced to approximately 5 mm, while still increasing device sensitivity over five times. Research needs to follow up these preliminary findings and fabricate a sensor for testing.

Also, the electro-optic switch and modulator described in the second and third publications of Chapter 4 [McCosker and Town, 2010d,c] should also be fabricated and tested.

Finally, research needs to determine whether the delta-κ configuration offers any advantages, such as during the fabrication process. For example, the fact that the electro-optic material is deposited around the MCDC waveguides may offer the advantage that

the waveguides can be deposited using an established technique for high accuracy and low side-wall roughness; whilst allowing the electro-optic material deposition to be carried out using a less accurate technique.

Bibliography

Ahmed, M. J. and Young, L. (1983). Mach-Zehnder interferometer tuning with Ta_2O_5 film loading. *Applied Optics*, 22:4082–4087.

Almeida, V. R., Xu, Q., Barrios, C. A., and Lipson, M. (2004). Guiding and confining light in void nanostructure. *Optics Letters*, 29:1209–1211.

Ando, S. (2004). Optical properties of fluorinated polyimides and their applications. *Journal of Photopolymer Science and Technology*, 17:219–232.

Barker, A. S. and Loudon, R. (1967). Dielectric properties and optical phonons in $LiNbO_3$. *Physics Review*, 158:433–445.

Barrios, C. A. (2009). Optical slot-waveguide based biochemcal sensors. *Sensors*, 9:4751–4765.

Barrios, C. A., Glyfason, K. B., Sánchez , B., Griol, A., Sohlström, H., Holgado, and Casquel, R. (2007). Slot-waveguide biochemical sensor. *Optics Letters*, 32:3080–3082.

Bergman, I. (1968). Rapid response atmospheric oxygen monitor based on fluorescence quenching. *Nature*, 218:396.

Brunner, F. D., Kwon, O.-P., Kwon, S.-J., Jazbinšek, M., Schneider, A., and Günter, P. (2008). A hydrogen-bonded organic nonlinear optical crystal for high-efficiency terahertz generation and detection. *Optics Express*, 16:16496–16508.

Bulmer, C. H., Burns, W. K., and Moeller, R. P. (1980). Linear interferometric waveguide modulator for electromagnetic-field detection. *Optics Letters*, 5:176–178.

Cho, S.-H., Lu, H. M., Cauller, L.and Romero-Ortega, M., Lee, J.-B., and Hughes, G. (2008). Biocompatible SU-8-based microprobes for recording neural spike signals from regenerated peripheral nerve fibers. *IEEE Sensors Journal*, 18:1830–1836.

Cleary, A., Garcia-Blanco, S., Glidle, A., Aitchison, J., Laybourn, P., and Cooper, J. (2005). An integrated fluorescence array as a platform for lab-on-a-chip technology using multimode interference splitters. *IEEE Sensors Journal*, 5:1315–1320.

Cooper, M. L. and Mookherjea, S. (2009). Numerically-assisted coupled-mode theory for silicon waveguide couplers and arrayed waveguides. *Optics Express*, 17:1583–1599.

Culshaw, B. (2004). Optical fiber sensor technologies. *Journal of Lightwave Technology*, 22:39.

Dalton, L. R., Robinson, B. H., Jen, A. K.-Y., Reid, P., Eichinger, B., Jang, S.-H., Luo, J., Liao, Y., Firestone, K. A., Bhatambrekar, N. P., Bale, D., Haller, M. A., Bhattacharjee, S., Schendel, J., Sullivan, P. A., Hammond, S., Buker, N., Cady, F., Chen, A., and Steier, W. H. (2004). Organic electro-optic materials. *Proceedings of the SPIE*, 5621:93–105.

Dalton, L. R., Sullivan, P. A., and Bale, D. H. (2010). Electric field poled organic electro-optic materials: State of the art and future prospects. *Chemical Reviews*, 110:25–55.

Dell'Olio, F. and Passaro, V. M. N. (2007). Optical sensing by optimized silicon slot waveguides. *Optics Express*, 15:4977–4993.

Demchenko, A. P. (2008). *Introduction to fluorescence sensing*. Springer.

Dinesen, P. G., Rasmussen, T., Lester, C., and Bjarklev, A. (1996). Microwave characteristics of polymer electro-optic modulators. *Applied Optics*, 35:4124.

Ebeling, K. J. (2003). *Integrated Optoelectronics: Waveguide Optics, Photonics, Semiconductors*. Springer-Verlag Berlin.

Efremidis, N. K. and Christodoulides, D. N. (2005). Revivals in engineered waveguide arrays. *Optics Communications*, 246:345–356.

Eggins, B. R. (2002). *Chemical sensors and biosensors*. Wiley.

Enami, Y., Derose, C. T., Mathine, D., Loychik, C., Greenlee, C., Norwood, R. A., Kim, T. D., Luo, J., Tian, Y., Jen, A. K.-Y., and Peyghambarian, N. (2007). Hybrid polymer/sol-gel waveguide modulators with exceptionally large electro-optic coefficients. *Nature Photonics*, 1:180–185.

Esinenco, D., Psoma, S., Kusko, M., Schneider, A., and Muller, R. (2005). SU-8 microbiosensor based on Mach-Zehnder interferometer. *Reviews on Advanced Materials Science*, 10:295–299.

Fan, X., White, I. M., Shopova, S. I., Zhu, H., Jonathan D, S., and Sun, Y. (2008). Sensitive optical biosensors for unlabeled targets: A review. *Analytica Chimica Acta*, 620:8–26.

Fang, Y. (2007). Non-invasive optical biosensor for probing cell signaling. *Sensors*, 7:2316–2329.

Feng, N.-N., Michel, J., and Kimerling, L. C. (2006). Optical field concentration in low-index waveguides. *IEEE Journal of Quantum Electronics*, 42:885–890.

Fini, J. M. (2004). Microstructure fibres for optical sensing in gases and liquids. *Measurement Science and Technology*, 15:11201128.

Fogli, F., Saccomandi, L., Bassi, P., Bellanca, G., and Trillo, S. (2002). Full vectorial BPM modeling of index-guiding photonic crystal fibers and couplers. *Optics Express*, 10:54–59.

Gallagher, D. (2008). Photonic CAD matures. *IEEE LEOS NewsLetter*.

Gallagher, D. F. G. and Felici, T. P. (2003). Eigenmode expansion methods for simulations of optical propagation in photonics - pros and cons. *Proceedings of the SPIE*, 4987:69–82.

Harsányi, G. (2000). *Sensors in biomedical applications: Fundamentals, technology & applications*. CRC Press.

Hautefeuillea, M., O'Mahonyb, C., O'Flynnb, B., Khalfib, K., and Peters, F. (2008). A MEMS-based wireless multisensor module for environmental monitoring. *Microelectronics Reliability*, 48:906–910.

Henry, W. M. and Payne, F. P. (1995). Solid-state tapered optical fibre devices. *Optical and Quantum Electronics*, 27:185–191.

Hong, J.-K., Lee, S.-S., and S.-S., L. (2007). Extraneous self-imaging phenomenon with weak-guiding condition. *Optics Letters*, 32:1311–1313.

Horváth, R., Lindvold, L., and Larsen, N. (2002). Reverse-symmetry waveguides: Theory and fabrication. *Applied Physics B*, 74(4):383–393.

Horváth, R., Pedersen, H. C., Skivesen, N., Selmeczi, D., and Larsen, N. B. (2003). Optical waveguide sensor for on-line monitoring of bacteria. *Optics Letters*, 28:1233–1235.

Howerton, M. M., Bulmer, C. H., and Burns, W. K. (1988). Linear 1×2 directional coupler for electromagnetic field detection. *Applied Physics Letters*, 52:1850–1852.

Hua, P., Luff, B. J., Quigleya, G. R., and Kawaguchi, J. S. W. K. (2002). Integrated optical dual Mach-Zehnder interferometer sensor. *Sensors and Actuators B*, 87:250–257.

Huanga, M.-S., Lu, M.-H., and Shy, J.-T. (2004). High sensitivity bulk electro-optic modulator field sensor for high voltage environments. *Review of Scientific Instruments*, 75:5364.

Hug, T. S., Prenosil, J. E., Maier, P., and Morbidelli, M. (2002). Optical waveguide lightmode spectroscopy (OWLS) to monitor cell proliferation quantitatively. *Biotechnology and Bioengineering*, 80:213–221.

Hunsperger, R. G. (2009). *Integrated Optics: Theory and Technology*. Springer.

Hunziker, C., Jazbinšek, M., Kwon, S.-J., Kwon, O.-P., Figi, H., and Günter, P. (2009). Electro-optic modulation in high-efficiency crystalline OH1 optical waveguides. In *Conference on Quantum Electronics and Laser Science Conference (CLEO/QELS)*.

Hunziker, C., Kwon, S.-J., Figi, H., Jazbinšek, M., and Günter, P. (2008a). Fabrication and phase modulation in organic single-crystalline configurationally locked, phenolic polyene OH1 waveguides. *Optics Express*, 16:15903.

Hunziker, C., Kwon, S.-J., Figi, H., Juvalta, F., Kwon, O.-P., Jazbinšek, M., and Günter, P. (2008b). Configurationally locked, phenolic polyene organic crystal 2-{3-(4-hydroxystyryl)-5, 5-dimethylcyclohex-2-enylidene} malononitrile: Linear

and nonlinear optical properties. *Journal of the Optical Society of America B*, 25:1678–1683.

Iwanow, R., May-Arrioja, D. A., Christodoulides, D. N., Stegeman, G. I., Min, Y., and Sohler, W. (2005). Discrete talbot effect in waveguide arrays. *Physical Review Letters*, 95:053902.

Jaeger, N. A. F. and Young, L. (1989). High-voltage sensor employing an integrated optics Mach-Zehnder interferometer in conjunction with a capacitive divider. *Journal of Lightwave Technology*, 7:229 – 235.

Jazbinšek, M., Mutter, L., and Günter, P. (2008). Photonic applications with the organic nonlinear optical crystal DAST. *IEEE Journal of Selected Topics in Quantum Electronics*, 14:1298–1311.

Kapon, E., Katz, J., and Yariv, A. (1984). Supermode analysis of phase-locked arrays of semiconductor lasers. *Optics Letters*, 9:125–127.

Kobayashi, T., Mari, S., Koshiishi, M., Nimomiya, K., Matsuki, M., Yokoyama, H., and Hara, T. (1984). Development of compact 500-kV 8000-A gas insulated transmission line study on insulation design. *IEEE Transactions on Power Apparatus and Systems*, PAS-103:3154–3162.

Kolev, T., Glavcheva, Z., Yancheva, D., Schúrmann, M., Kleb, D. C., Preut, H., and Bleckmann, P. (2001). 2-3-[2-(4-Hydroxyphenyl)vinyl]-5,5-dimethylcyclohex-2-en-1-ylidenemalononitrile. *Acta Crystallographica*, E57:o561–o562.

Kondo, J., Kondo, A., Aoki, K., Imaeda, M., Mori, T., Mizuno, Y., Takatsuji, S., Kozuka, Y., Mohapatra, O. S. K., Francis, C. V., Hahn, K., and Dolfi, D. W. (1993). Mi-

crowave loss in nonlinear optical polymers. *Journal of Applied Physics*, 73:2569–2571.

Kribich, K. R., Copperwhite, R., Barry, H., Kolodziejczyk, B., Sabattie, J.-M., O'Dwyer, K., and MacCraith, B. D. (2004). Novel chemical sensor/biosensor platform based on optical multimode interference (MMI) couplers. *Sensors and Actuators B*, 107:188–192.

Kuhlmey, B. T., Eggleton, B. J., and Wu, D. K. C. (2009). Fluid-filled solid-core photonic bandgap fibers. *Journal of Lightwave Technology*, 27:1617–1630.

Kwon, O.-P., Kwon, S.-J., Jazbinšek, M., Brunner, F. D. J., Seo, J.-I., Hunziker, C., Schneider, A., Yun, H., Lee, Y.-S., and Günter, P. (2008). Organic phenolic configurationally locked polyene single crystals for electro-optic and terahertz wave applications. *Advanced Functional Materials*, 18:3242–3250.

Lee, B. (2003). Review of the present status of optical fiber sensors. *Optical Fiber Technology*, 9:57–59.

Lee, M., Katz, H. E., Erben, C., Gill, D. M., Gopalan, P., Heber, J. D., and McGee, D. J. (2002a). Broadband modulation of light by using an electro-optic polymer. *Science*, 282:1401–1403.

Lee, M., Mitrofanov, O., Katz, H. E., and Erben, C. (2002b). Millimeter-wave dielectric properties of electro-optic polymer materials. *Applied Physics Letters*, 81:1474.

Lee, S. S., Oh, M. C., Shin, S. Y., and Keh, K. H. (1993). Integrated optical high-voltage sensing using z-cut $LiNbO_3$ cutoff modulator. *IEEE Photonics Technology Letters*, 5:996.

Lemke, R. (1970). Different alcohols. *Chemische Berichte*, 103:1894–1899.

Lippitsch, M. E., Draxler, S., Kieslinger, D., Lehmann, H., and Weigl, B. H. (1996). Capillary waveguide optrodes: An approach to optical sensing in medical diagnostics. *Applied Optics*, 35:3426–3431.

Liu, J.-M. (2005). *Photonic Devices*. Cambridge University Press.

Luff, B. J., Harris, R. D., Wilkinson, J. S., Wilson, R., and Schiffrin, D. J. (1996). Integrated-optical directional coupler biosensor. *Optics Letters*, 21(8):618–620.

Luff, B. J., Wilkinson, J. S., Piehler, J., Hollenback, U., Ingenhoff, J., and Fabricius, N. (1998). Integrated Mach-Zehnder biosensor. *Journal of Lightwave Technology*, 16:583–592.

Lukosz, W. and Tiefenthaler, K. (1983). Directional switching in planar waveguides effected by absorption-desorption processes. In *Proceedings of the 2nd European Conference of Integrated Optics*, volume 227, pages 152–155, Florence, Italy.

Mangan, B. (2000). Experimental study of dual-core photonic crystal fibre. *Electronics Letters*, 36:1358.

Manz, A., Graber, N., and Widmer, H. M. (1990). Miniaturized total chemical-analysis systems: A novel concept for chemical sensing. *Sensors and Actuators B*, 1:244–248.

Martelli, C., abd M. Kristensen, J. C., and Groothoff, N. (2007). Refractive index measurement within a photonic crystal fibre based on short wavelength diffraction. *Sensors*, 7:2492–2498.

McCosker, R. J. and Town, G. (2010a). An electro-optic modulator using a multichannel directional coupler with a poled electro-optic polymer. In *Proceedings*

of the Third International Conference on Communications and Electronics (ICCE), Nha Trang, pages 329–334.

McCosker, R. J. and Town, G. (2010b). Optical chemical sensor using a multi-channel directional coupler with slot waveguides. In *Proceedings of the International Conference on Photonics (ICP), Langkawi*, pages 1–5.

McCosker, R. J. and Town, G. E. (2009). Electric field sensor based on a multi-channel directional-coupler with an electro-optic polymer. In *Proceedings of the 34th Australian Conference on Optical Fibre Technology (ACOFT), Adelaide*, pages 481–482.

McCosker, R. J. and Town, G. E. (2010c). A delta-k electro-optic polymer modulator using a multi-channel directional coupler. In *Proceedings of the International Conference on Electromagnetics in Advanced Applications (ICEAA), Sydney*, pages 859–862.

McCosker, R. J. and Town, G. E. (2010d). An electro-optic switch based on a multi-channel directional coupler. In *Proceedings of the 35th Australian Conference on Optical Fibre Technology (ACOFT), Melbourne*.

McCosker, R. J. and Town, G. E. (2010e). Multi-channel directional coupler as an evanescent field optical sensor. *Sensors and Actuators B*, 150:417–424.

McCosker, R. J. and Town, G. E. (2010f). Multi-channel directional coupler for WDM in fluorescence sensing. *submitted to IEEE Photonic Technology Letters*.

McCosker, R. J. and Town, G. E. (2010g). Optical chemical sensor using a differential multi-channel directional coupler with slot waveguides. *submitted to Sensors and Actuators B*.

McCosker, R. J. and Town, G. E. (2010h). Optical electric field sensor using a multi-channel directional coupler. *submitted to IEEE Sensors Journal*.

McCosker, R. J. and Town, G. E. (2010i). Partial image revivals in a multi-channel directional-coupler. *Proceedings of the SPIE*, 7604:76040G.

Moerner, W. E. (2007). New directions in single-molecule imaging and analysis. *Proceedings of the National Academy of Sciences*, 104:12596–602.

Monro, T. M., Belardi, W., Furusawa, K., Baggett, J. C., Broderick, N. G. R., and Richardson, D. J. (2001). Sensing with microstructured optical fibres. *Measurement Science and Technology*, 12:854.

Moreau, W. M. (1988). *Semiconductor Lithography-Principles*. Plenum, New York.

Naghski, D. H., Boyd, J. T., Jackson, H., Sriram, S., Kingsley, S. A., and Latess, J. (1994). An integrated photonic Mach-Zehnder interferometer with no electrodes for sensing electric field. *Journal of Lightwave Technology*, 12:1092 – 1098.

Narayanaswamy, R. and Wolfbeis, O. (2004). *Optical Sensors: Industrial, Environmental and Diagnostic Applications Series*. Springer, Heidelberg.

Nicolas, A., Jaeger, F., and Young, L. (1987). Asymmetric slab and strip-loaded integrated optic devices for the measurement of large electric fields. *Journal of Lightwave Technology*, 5:745–750.

Nordstrom, M., Zauner, D., Boisen, A., and Hubner, J. (2007). Single-mode waveguides with SU-8 polymer core and cladding for MOEMS applications. *Journal of Lightwave Technology*, 25(5):1284–1289.

Parriaux, O. and Veldhuis, G. (1998). Normalized analysis for the sensitivity optimization of integrated optical evanescent-wave sensors. *Journal of Lightwave Technology*, 16:573 –582.

Passaro, V. M. N., Dell'Olio, F., Casamassima, B., and De Leonardis, F. (2007). Guided-wave optical biosensors. *Sensors*, 7:508–536.

Passaro, V. M. N., Dell'Olio, F., Ciminelli, C., and Armenise, M. N. (2009). Efficient chemical sensing by coupled slot SOI waveguides. *Sensors*, 9:1012–1032.

Passaro, V. M. N., Dell'Olio, F., and Leonardis, F. D. (2006). Electromagnetic field photonic sensors. *Progress in Quantum Electronics*, 30:45–73.

Pohanka, M., Skladal, P., and Kroca, M. (2007). Biosensors for biological warfare agent detection. *Defence Science Journal*, 57(3):185–193.

Poon, J. K. S., Huang, Y., Paloczi, G. T., and Yariv, A. (2004). Wide-range tuning of polymer microring resonators by the photobleaching of CLD-1 chromophores. *Optics Letters*, 29:2584–2586.

Rahmatian, F. and Blake, J. N. (2006). Applications of high-voltage fiber optic current sensors. *IEEE PES General Meeting*.

Rezzonico, D., Kwon, S. J., Figi, H., Kwon, O., Jazbinsek, M., and Guunter, P. (2008). Photochemical stability of nonlinear optical chromophores in polymeric and crystalline materials. *Journal of Chemical Physics*, 128:124713.

Rindorf, L., Hiby, P. E., Jensen, J. B., Pedersen, L. H., Bang, O., and Geschke, O. (2006). Towards biochips using microstructured optical fiber sensors. *Analytical and Bioanalytical Chemistry*, 385:1370–1375.

Ritari, T., Tuominen, J., Ludvigsen, H., Petersen, J., Srensen, T., Hansen, T., and Simonsen, H. (2004). Gas sensing using air-guiding photonic bandgap fibers. *Optics Express*, 12:4080–4018.

Runde, D., Brunken, S., Rüter, C. E., and Kip, D. (2007). Integrated optical electric field sensor based on a Bragg grating in lithium niobate. *Applied Physics B*, 86:91–95.

Russell, P. (2003). Photonic crystal fibers. *Science*, 299:358–362.

Saitoh, K., Sato, Y., and Koshiba, M. (2003). Coupling characteristics of dual-core photonic crystal fiber couplers. *Optics Express*, 11:3188–3195.

Schipper, E., Brugman, A., Dominguez, C., Lechuga, L., Kooyman, R., and Greve, J. (1997). The realization of an integrated Mach-Zehnder waveguide immunosensor in silicon technology. *Sensors and Actuators B*, 40:147–153.

Schmitt, K., Schirmer, B., Hoffmann, C., Brandenburg, A., and Meyrueis, P. (2007). Interferometric biosensor based on planar optical waveguide sensor chips for label-free detection of surface bound bioreactions. *Biosensors and Bioelectronics*, 22:2591–2597.

Shi, Y., Lin, W., Olson, D. J., and Bechtel, J. H. (2000a). Electro-optic polymer modulators with 0.8 V half-wave voltage. *Applied Physics Letters*, 77:1–3.

Shi, Y., Wang, W., Lin, W., Olson, D. J., and Bechtel, J. H. (1997). Long-term stable direct current bias operation in electro-optic polymer modulators with an electrically compatible multilayer structure. *Applied Physics Letters*, 71:2236.

Shi, Y. Q., Zhang, C., Zhang, H., Bechtel, J. H., Dalton, L. R., Robinson, B. H., and Steier,

W. H. (2000b). Low (sub-1-volt) halfwave voltage polymeric electro-optic modulators achieved by controlling chromophore shape. *Science*, 288:119–122.

Silin, V. I., Balchytis, G. A., and Kulys, J. J. (1993). The application of polystyrene waveguides to protein absorption investigations. *Journal of Biochemical and Biophysical Methods*, 26:71–79.

Soldano, L. B. and Pennings, E. C. M. (1995). Optical multi-mode interference devices based on self-imaging: Principles and applications. *Journal of Lightwave Technology*, 13:615–627.

Somekh, S., Garmire, E., Yariv, A., Garvin, H. L., and Hunsperger, R. G. (1973). Channel optical waveguide directional couplers. *Applied Physics Letters*, 22:46–47.

Somekh, S. R. (1974). *Theory, fabrication and performance of some integrated optical devices*. PhD thesis, California Institute of Technology, California.

Soref, R. A., Schimidtchen, J., and Petermann, K. (1991). Large single-mode rib waveguides in GeSi-Si and Si-on-SiO_2. *IEEE Journal of Quantum Electronics*, 127:1971–1974.

Stewart, G. and Culshaw, B. (1994). Optical waveguide modeling and design for evanescent field chemical sensors. *Optical and Quantum Electronics*, 26:S249–S259.

Thapliya, R., Nakamura, S., and Kikuchi, T. (2006). Electro-optic multimode interference device using organic materials. *Applied Optics*, 45:5404–5413.

Thrush, E., Levi, O., Cook, L. J., Deich, J., Kurtz, A., Smith, S. J., Moerner, W., and Jr., J. S. H. (2005). Monolithically integrated semiconductor fluorescence sensor for microfluidic applications. *Sensors and Actuators B*, 105:393–399.

Town, G. E., Copperwhite, R., Kribich, R., O'Dwyer, K., and MacCraith, B. (2005). Comparison of multimode and multichannel couplers for evanescent wave sensing of refractive index. In *Proceedings of the 30th Australian Conference on Optical Fibre Technology (ACOFT), Sydney*.

Town, G. E., McCosker, R., Yuan, W., and Bang, O. (2010a). Design of microstructured waveguide devices for applications in optical sensing. In *Proceedings of the Optics & Photonics Congress, Advanced Photonics & Renewable Energy, Karlsruhe*.

Town, G. E., Yuan, W., McCosker, R., and Bang, O. (2010b). Microstructured optical fiber refractive index sensor. *Optics Letters*, 35:856–858.

Turner, E. H. (1966). The far infrared optical properties of $LiNbO_3$. *Applied Physics Letters*, 8:303–304.

van Eijkelenborg, M. A., Argyros, A., Barton, G., Bassett, I. M., Fellew, M., Henry, G., Issa, N. A., Large, M. C. J., Manos, S., Padden, W., Poladian, L., and Zagari, J. (2003). Recent progress in microstructured polymer optical fibre fabrication and characterisation. *Optical Fiber Technology*, 9:199–209.

Vengsarkar, A., Lemaire, P. J., Judkins, J. B., Bhatia, V., Erdogan, T., and Sipe, J. E. (1996). Long-period fiber gratings as band-rejection filters. *Journal of Lightwave Technology*, 14:58–65.

Wang, X., Li, B., Xiao, Z., Lee, S. H., Roman, H., Russo, O. L., Chin, K. K., and Farmer, K. R. (2005). An ultra-sensitive optical MEMS sensor for partial discharge detection. *Journal of Micromechanics and Microengineering*, 15:521–527.

Weiss, S. M. (2006). Porous silicon waveguide biosensors. In *LEOS Annual Meeting Conference, Montreal*.

Wong, K. K. (2002). *Properties of lithium niobate*. The Institution of Engineering and Technology.

Xia, Y. and Whitesides, G. M. (1998). Soft lithography. *Annual Review of Materials Research*, 28:153184.

Xu, F., Pruneri, V., Finazzi, V., and Brambilla, G. (2008). An embedded optical nanowire loop resonator refractometric sensor. *Optics Express*, 16:1062–1067.

Yariv, A. (1973). Coupled-mode theory for guided-wave optics. *IEEE Journal of Quantum Electronics*, 9:19–33.

Yariv, A. (1997). *Optical Electronics in Modern Communications*. Oxford University Press, New York.

Yariv, A. and Yeh, P. (2007). *Photonics: Optical Electronics in Modern Communications (6th Ed.)*. Oxford Univiversity Press, New York.

Yuan, W., Town, G., and Bang, O. (2010). Refractive index sensing in an all-solid twin-core photonic bandgap fiber. *IEEE Sensors Journal*, 10:1192–1199.

Zeng, R., Zhang, Y., Chen, W., and Zhang, B. (2008). Measurement of electric field distribution along composite insulators by integrated optical electric field sensor. *IEEE Transactions on Dielectrics and Electrical Insulation*, 15:302 –310.

Zhang, C., Dalton, L. R., Oh, M.-C., Zhang, H., and Steier, W. H. (2001). Low Vπ electrooptic modulators from CLD-1: Chromophore design and synthesis, material processing and characterization. *Chemistry of Materials*, 13:3042–3050.

Zhi, L., Zhou, H.-F., Yang, J.-Y., and Jiang, X.-Q. (2008). Talbot effect in three waveguide arrays. *Chinese Physics Letters*, 25:3307–3310.

Electro-optic Theory

A.1 Dielectric Tensor

In the absence of an applied electric field for a linear anisotropic medium, there is a unique set of coordinate axes for which the dielectric tensor $\boldsymbol{\varepsilon}(\omega)$ is diagonal. These unique coordinate axes $(\hat{x}, \hat{y}, \hat{z})$ are called the principal dielectric axes or simply principal axes of the dielectric material. Along the directions of these principle axes the $\boldsymbol{D}$ and $\boldsymbol{E}$ field vectors are parallel, and their components have the following relations:

$$D_x = \varepsilon_x E_x, \quad D_y = \varepsilon_y E_y, \quad D_z = \varepsilon_z E_z. \tag{A.1.1}$$

In this coordinate system, the dielectric tensor $\boldsymbol{\varepsilon}(\omega)$ is given by

$$\boldsymbol{\varepsilon}(\omega) = \begin{bmatrix} \varepsilon_x & 0 & 0 \\ 0 & \varepsilon_y & 0 \\ 0 & 0 & \varepsilon_z \end{bmatrix}, \tag{A.1.2}$$

where $\boldsymbol{\varepsilon}$ is symmetric, i.e. $\varepsilon_{ij} = \varepsilon_{ji}$. The dielectric tensor $\boldsymbol{\varepsilon}$ is diagonalised with eigenvalues ε_x, ε_y and ε_z, which can also define three principal indices of refraction as

$$n_x = \sqrt{\frac{\varepsilon_x}{\varepsilon_0}}, \quad n_y = \sqrt{\frac{\varepsilon_y}{\varepsilon_0}}, \quad n_z = \sqrt{\frac{\varepsilon_z}{\varepsilon_0}}. \tag{A.1.3}$$

In the presence of an applied electric field $\mathbf{E}_0$ the electro-optically induced changes usually result in changes to both the diagonal elements and the generation of off-diagonal elements. This nondiagonal dielectric tensor $\varepsilon(\omega, \mathbf{E}_0)$ is given by

$$\varepsilon(\omega, \mathbf{E}_0) = \begin{bmatrix} \varepsilon_x + \Delta\varepsilon_{xx} & \Delta\varepsilon_{xy} & \Delta\varepsilon_{xz} \\ \Delta\varepsilon_{yx} & \varepsilon_y + \Delta\varepsilon_{yy} & \Delta\varepsilon_{yz} \\ \Delta\varepsilon_{zx} & \Delta\varepsilon_{zy} & \varepsilon_z + \Delta\varepsilon_{zz} \end{bmatrix}. \tag{A.1.4}$$

The electro-optically induced nondiagonal dielectric tensor $\varepsilon(\omega, \mathbf{E}_0)$ can be diagonalised through a transform of coordinate axes. Alternatively, an equivalent method that involves a coordinate transform by rotation in the so-called index ellipsoid can be performed to eliminate cross-product terms.

A.2 Index Ellipsoid

The inverse of the dielectric tensor ε is the relative impermeability tensor η defined as

$$\eta = \left[\eta_{ij}\right] = \left(\frac{\varepsilon}{\varepsilon_0}\right)^{-1}, \tag{A.2.1}$$

where i and j are spatial coordinate indices. In a general rectangular system (x_1, x_2, x_3), the ellipsoid defined by

$$\sum_{i,j} x_i \eta_{ij} x_j = 1 \tag{A.2.2}$$

is called the index ellipsoid. Considering that ε is symmetric and therefore η is also symmetric then we can expand the index ellipsoid to be written as

$$\eta_{11}x_1^2 + \eta_{22}x_2^2 + \eta_{33}x_3^2 + 2\eta_{23}x_2x_3 + 2\eta_{31}x_3x_1 + 2\eta_{12}x_1x_2 = 1\,. \tag{A.2.3}$$

However, it is more convenient to introduce contracted indices to abbreviate the notation, which are defined as

$$\begin{aligned} &1 = (11);\ 2 = (22);\ 3 = (33);\\ &4 = (23) = (32);\ 5 = (31) = (13);\ 6 = (12) = (21). \end{aligned} \tag{A.2.4}$$

Thus the index ellipsoid is usually written as

$$\eta_1x_1^2 + \eta_2x_2^2 + \eta_3x_3^2 + 2\eta_4x_2x_3 + 2\eta_5x_3x_1 + 2\eta_6x_1x_2 = 1\,. \tag{A.2.5}$$

The index ellipsoid is invariant with respect to coordinate rotation. If a coordinate system is selected where its principle axes (x, y, z) coincide with the principal dielectric axes then the tensor η is diagonalised with the eigenvalues

$$\eta_x = \frac{\varepsilon_0}{\varepsilon_x} = \frac{1}{n_x^2};\quad \eta_y = \frac{\varepsilon_0}{\varepsilon_y} = \frac{1}{n_y^2};\quad \eta_z = \frac{\varepsilon_0}{\varepsilon_z} = \frac{1}{n_z^2}; \tag{A.2.6}$$

and the index ellipsoid can be simplified to

$$\frac{x^2}{n_x^2} + \frac{y^2}{n_y^2} + \frac{z^2}{n_z^2} = 1\,, \tag{A.2.7}$$

where the principal refractive indices n_x, n_y and n_z are given by the semiaxes (radii) of the index ellipsoid.

A.3 Relative Permeability Tensor

Electro-optically induced changes as a result of an applied electric field $\boldsymbol{E}$ are traditional defined in terms of changes to the relative permeability tensor $\boldsymbol{\eta}$ as

$$\boldsymbol{\eta}(\boldsymbol{E}) = \boldsymbol{\eta}(0) + \Delta\boldsymbol{\eta}(\boldsymbol{E}), \tag{A.3.1}$$

where $\boldsymbol{\eta}(0)$ is the field-independent component.

In this work, we only consider the first-order electro-optic effect, which is known as the Pockels effect or the linear electro-optic effect since it is characterised by the linear dependence of the elements of the relative permeability tensor $\eta_{ij}(\boldsymbol{E})$ on $\boldsymbol{E}$ through the coefficients r_{ijk}. It is assumed that higher-order electro-optic effects such as the Kerr effect are non-existent. Subsequently, we can expand the changes to Eq. A.3.1 in terms of the changes in the elements of $\boldsymbol{\eta}$ as

$$\eta_{ij}(\boldsymbol{E}) = \eta_{ij} + \Delta\eta_{ij}(\boldsymbol{E}) = \eta_{ij} + \sum_k r_{ijk}E_k, \tag{A.3.2}$$

where $\eta_{ij} = \eta_{ij}(0)$ and E_k is the k component of the electric field. The indices i and j are associated with optical fields, while indice k is associated with the low-frequency applied electric field. Since the impermeability tensor $\boldsymbol{\eta}$ is symmetric, i.e. $\eta_{ij} = \eta_{ji}$ then the linear electro-optic coefficients are also symmetric, i.e. $r_{ijk} = r_{kji}$. In this case, the index notation can be abbreviated using the contracted indices notation of Eq. A.2.4, where $\eta_\alpha = \eta_{ij}$ and $r_{\alpha k} = r_{ijk}$ and $\alpha = 1, 2, ..., 6$; as defined in Eq. A.2.4. Thus, Eq. A.3.2 is reduced to

$$\eta_\alpha(\boldsymbol{E}) = \eta_\alpha + \Delta\eta_\alpha(\boldsymbol{E}) = \eta_\alpha + \sum_k r_{\alpha k}E_k. \tag{A.3.3}$$

In the absence of an applied electric field, the index ellipsoid of a material is given by Eq. A.2.5 and has its principle axes aligned with $\hat{x}$, $\hat{y}$ and $\hat{z}$. The presence of an electric field $\boldsymbol{E}$ results in changes to the optical properties of the material. This is seen as a deformation of the index ellipsoid into a new one given by

$$\eta_{ij}(\boldsymbol{E})\, x_i x_j = 1 \tag{A.3.4}$$

or equivalently

$$\begin{aligned}&(\eta_1 + \Delta\eta_1)\, x^2 + (\eta_2 + \Delta\eta_2)\, y^2 + (\eta_3 + \Delta\eta_3)\, z^2 \\ &+2\Delta\eta_4 yz + 2\Delta\eta_5 zx + 2\Delta\eta_6 xy = 1\end{aligned} \tag{A.3.5}$$

whose principal axes no longer line up with $\hat{x}$, $\hat{y}$ and $\hat{z}$.

In order to diagonalise the new impermeability tensor $\boldsymbol{\eta}(\boldsymbol{E})$ and therefore the dielectric tensor $\boldsymbol{\varepsilon}(\boldsymbol{E})$, the cross-product terms yz, zx and xy must be eliminated. This is achieved through a coordinate transform by rotation in space of the index ellipsoid into

$$\frac{X^2}{n_X^2} + \frac{Y^2}{n_Y^2} + \frac{Z^2}{n_Z^2} = 1\,, \tag{A.3.6}$$

where the principal axes of the new ellipsoid are $\hat{X}$, $\hat{Y}$ and $\hat{Z}$.

A.4 Matrix Form of Pockels Coefficients

For the Pockels effect, the change in the permeability tensor is given by

$$\Delta\eta_\alpha = \sum_k r_{\alpha k} E_k\,, \tag{A.4.1}$$

which can be written in matrix form as

$$\begin{bmatrix} \Delta\eta_1 \\ \Delta\eta_2 \\ \Delta\eta_3 \\ \Delta\eta_4 \\ \Delta\eta_5 \\ \Delta\eta_6 \end{bmatrix} = \begin{bmatrix} r_{11} & r_{12} & r_{13} \\ r_{21} & r_{22} & r_{23} \\ r_{31} & r_{32} & r_{33} \\ r_{41} & r_{42} & r_{43} \\ r_{51} & r_{52} & r_{53} \\ r_{61} & r_{62} & r_{63} \end{bmatrix} \begin{bmatrix} E_x \\ E_y \\ E_z \end{bmatrix}, \tag{A.4.2}$$

where the 6×3 matrix with elements r_{ij} is called the electro-optic tensor.